



December 03, 2018

Docket No. 52-048

U.S. Nuclear Regulatory Commission
ATTN: Document Control Desk
One White Flint North
11555 Rockville Pike
Rockville, MD 20852-2738

SUBJECT: NuScale Power, LLC Response to NRC Request for Additional Information No. 136 (eRAI No. 8933) on the NuScale Design Certification Application

REFERENCES: 1. U.S. Nuclear Regulatory Commission, "Request for Additional Information No. 136 (eRAI No. 8933)," dated August 05, 2017
2. NuScale Power, LLC Supplemental Response to "NRC Request for Additional Information No. 136 (eRAI No. 8933)" dated October 3, 2018
3. NuScale Power, LLC Supplemental Response to "NRC Request for Additional Information No. 136 (eRAI No. 8933)" dated October 30, 2018

The purpose of this letter is to provide the NuScale Power, LLC (NuScale) response to the referenced NRC Request for Additional Information (RAI).

The Enclosure to this letter contains NuScale's response to the following RAI Question from NRC eRAI No. 8933:

- 03.07.02-17

A majority of the responses to RAI No. 136, eRAI No. 8933, questions were previously provided in References 2 and 3. This completes all responses to eRAI 8933.

This letter and the enclosed response make no new regulatory commitments and no revisions to any existing regulatory commitments.

If you have any questions on this response, please contact Marty Bryan at 541-452-7172 or at mbryan@nuscalepower.com.

Sincerely,

Zackary W. Rad
Director, Regulatory Affairs
NuScale Power, LLC

Distribution: Gregory Cranston, NRC, OWFN-8G9A
Samuel Lee, NRC, OWFN-8G9A
Marieliz Vera, NRC, OWFN-8G9A



RAIO-1218-63681

Enclosure 1: NuScale Response to NRC Request for Additional Information eRAI No. 8933



Enclosure 1:

NuScale Response to NRC Request for Additional Information eRAI No. 8933

Response to Request for Additional Information Docket No. 52-048

eRAI No.: 8933

Date of RAI Issue: 08/05/2017

NRC Question No.: 03.07.02-17

10 CFR 50 Appendix S requires that the safety functions of structures, systems, and components (SSCs) must be assured during and after the vibratory ground motion associated with the Safe Shutdown Earthquake (SSE) through design, testing, or qualification methods.

- a. Figure 3.7.2-13 in the FSAR indicates that the refueling area foundation is lower than the neighboring reactor pool and spent fuel pool area (which is also mentioned in the bottom paragraph on Page 3.7-24, indicating a six feet elevation difference). However, Figure 3.7.2-20 does not indicate these differences in foundation elevation. The applicant is requested to clarify whether these foundation elevation differences are taken into account in the RXB model; and, if not, please provide justification for not doing so.
- b. On Page 3.7-25 of the FSAR, in the sixth paragraph, the applicant states, “The rigid springs have a zero length and have a stiffness value large enough to simulate rigid connection. The large stiffness used is arbitrarily chosen to be ten billion lbs per inch, or 1010 lbs/inch, in the three global directions.” For the spring to be modeled as a rigid spring, the value of its spring constant should be sufficiently larger than the stiffness of the structural element (basemat) to which it is attached. The applicant is requested to confirm the adequacy of the number (1010 lbs/inch) chosen for the spring constant by comparing it to the stiffness of the adjacent basemat element or through an appropriate sensitivity run using a number at least an order of magnitude different.
- c. In Table 3.7.2-1 in the FSAR, the maximum aspect ratio for RXB finite elements is indicated as 11.9. The applicant is requested to ensure that this value of aspect ratio is within the range of the parameters covered in the SASSI V&V; if not, provide justification

for the adequacy of using the maximum aspect ratio of 11.9 for RXB finite elements.

NuScale Response:

a.

Figure 3.7.2-13 displays the south side of the reactor building (RXB), while Figure 3.7.2-20 displays the north side of the RXB, a section cut that does not include the refuel or spent fuel pool. The RXB model did not account for elevation differences in the refueling pool. The pits are designed as an integral part of the entire foundation design. The pits are necessary for plant operational and maintenance needs during refueling outages. The sides of the pit transition into the main foundation with sloped sides, which reduces the resistance during horizontal motion. The base areas of the pits are small compared to the overall foundation size. The bottom thicknesses of the pits are the same as the foundation thickness, 10 ft. Not including the foundation elevation difference in the structural model does not change the structural dynamics or response of the structure.

b.

A sensitivity analysis was performed by increasing the stiffness of the RXB rigid springs by an order of magnitude, to 10^{11} lb/in, and comparing results obtained from the base case, rigid spring stiffness = 10^{10} lb/in. For this study, the RXB model with cracked concrete properties, 7% concrete damping, Soil Type 7, and the Capitola input motion, was used. Comparisons of transfer functions or ISRS show that increasing the rigid spring stiffness has no discernible effect on the transfer functions or in-structure response spectra (ISRS).

Comparison of the sums of the maximum spring forces shows that the total changed by 0.17%. The average of the percent difference of the forces over all of the rigid spring elements is provided in Table 1-3. The largest average percent difference is 0.29%, in the X (EW) and Y (NS) directions.

Comparisons of the maximum stresses, forces, and moments in typical solid, beam, and shell elements are shown in below Section 1.4, Section 1.5, and Section 1.6, respectively. The average change over all of the elements is less than 0.3%.

Based on the results presented from this study, it can be concluded that the value of 10^{10} lb/in used for the spring constant is sufficient to model the soil springs connecting the RXB basemat and backfill to the freefield.

It should be noted that the results of this study also apply to the control building (CRB) SASSI model. This is because the same stiffness value of 10^{10} lb/in was used for the rigid springs in both the CRB and the RXB SASSI models, and the weight of the CRB is significantly less than that of the RXB.

1.1 Transfer Function Comparison

Transfer function (TF) comparisons are provided at the seven locations listed in Table 1-1. Transfer function comparisons at the lugs are only presented in the direction in which the lugs are restrained, that is, in the NS direction for the west and east lugs, and in the EW direction for the north and south lugs.

The locations of the nodes are shown in Figure 1-1 through Figure 1-4. The cracked concrete model with 7% concrete damping was used to generate these results. The TF comparisons are shown in Figure 1-5 through Figure 1-19. There are no discernible differences in the transfer functions between spring $K = 10^{10}$ lb/in and spring $K = 10^{11}$ lb/in.

Table 1-1. Locations of TF and ISRS Comparisons.

Node	X (in)	Y (in)	Z (in)	Description
3996	0.00	873.00	120.00	Northwest Corner on Top of Basemat
16257	1918.50	305.50	673.73	RXM 1 at West Lug Support Location
16271	2019.50	406.50	673.73	RXM 1 at North Lug Support Location
16287	2120.50	305.50	673.73	RXM 1 at East Lug Support Location
27649	1872.00	453.00	1548.00	Crane Rail Slab at Grid Line RX-4 at El. 145'-6"
27692	2328.75	453.00	1548.00	Crane Rail Slab between Grid Lines RX-4 and RX-5 at El. 145'-6"
30350	2019.50	0.00	1980.00	Roof Slab between Grid Lines RX-4 and RX-5

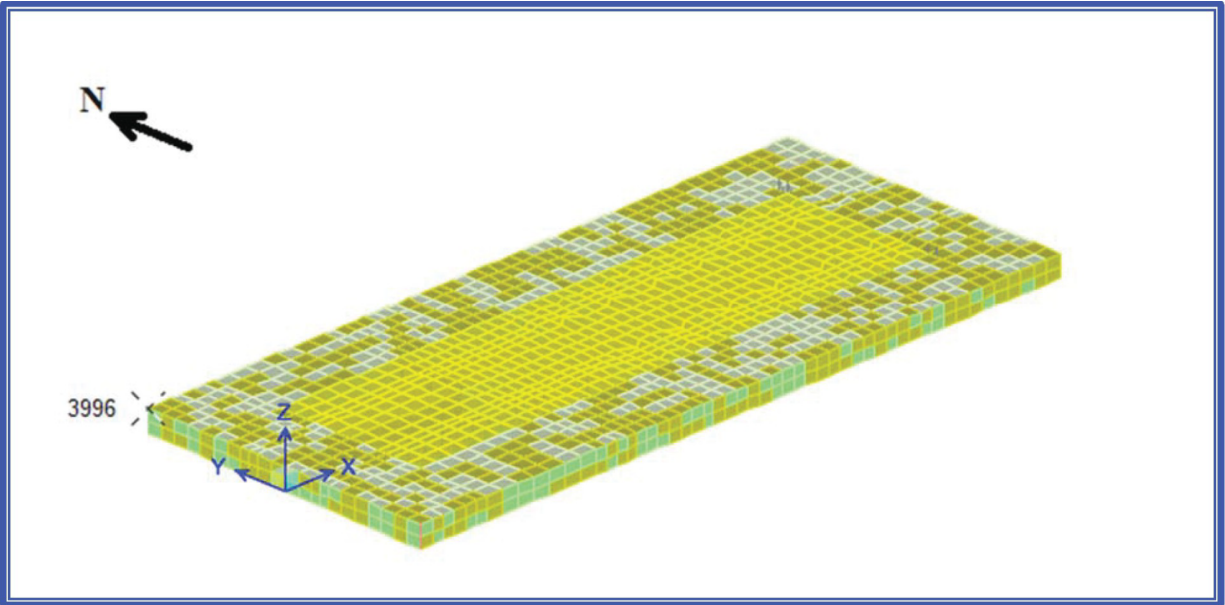


Figure 1-1. Node 3996, Northwest Corner on Top of Basemat.

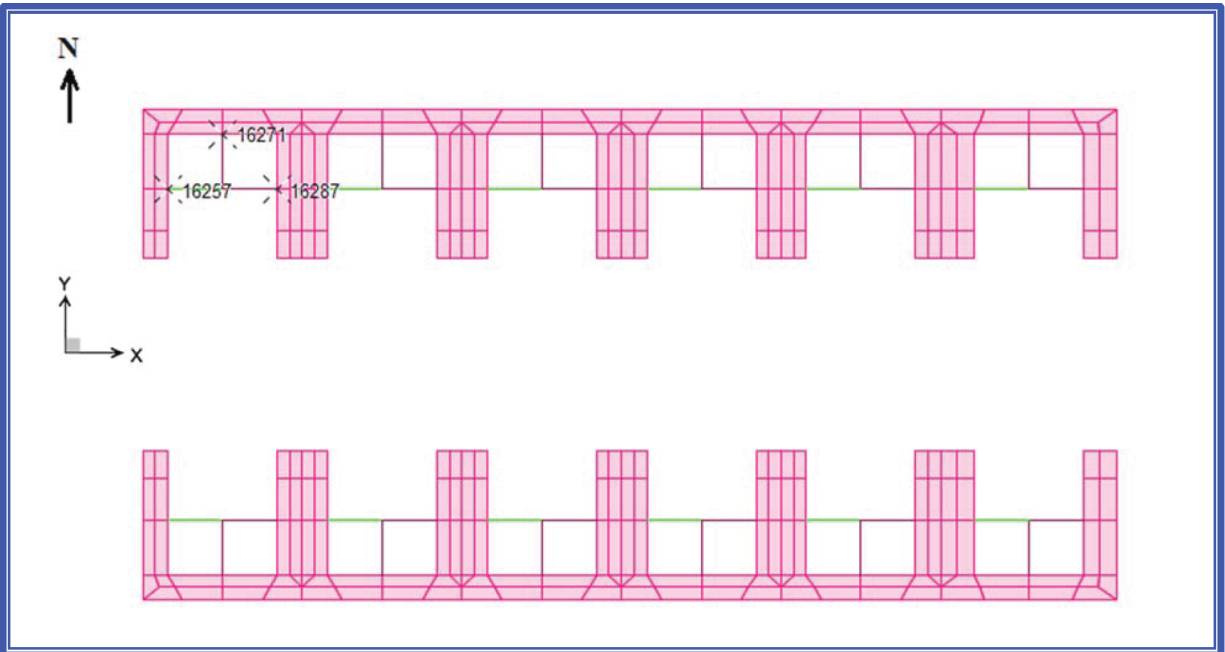


Figure 1-2. Node 16257 (West), Node 16271 (North), and Node 16287 (East) RXM 1 Lug Supports.

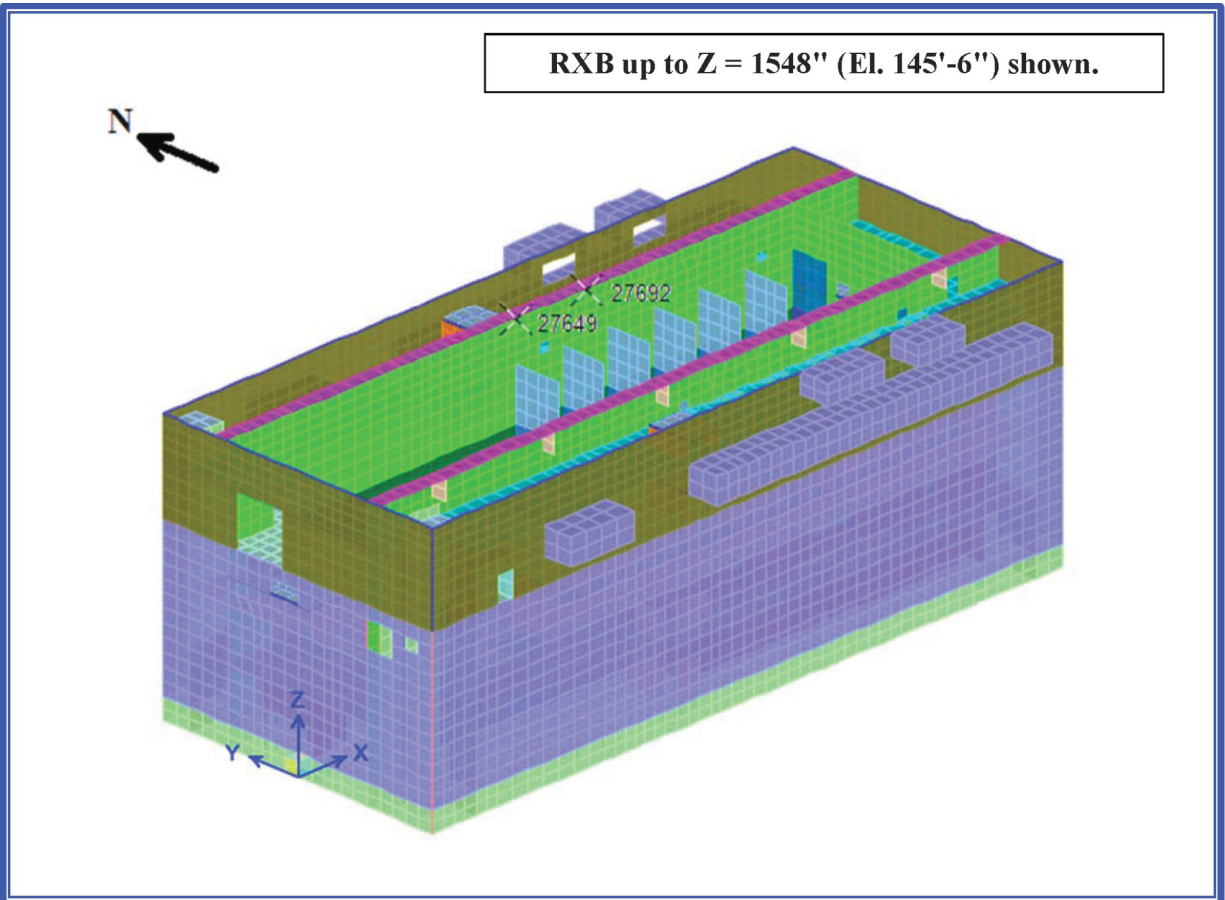


Figure 1-3. Node 27649 (Crane Rail Slab at Grid Line RX-4) and Node 27692 (Crane Rail Slab between Grid Lines RX4 and RX-5) at El. 145'-6".

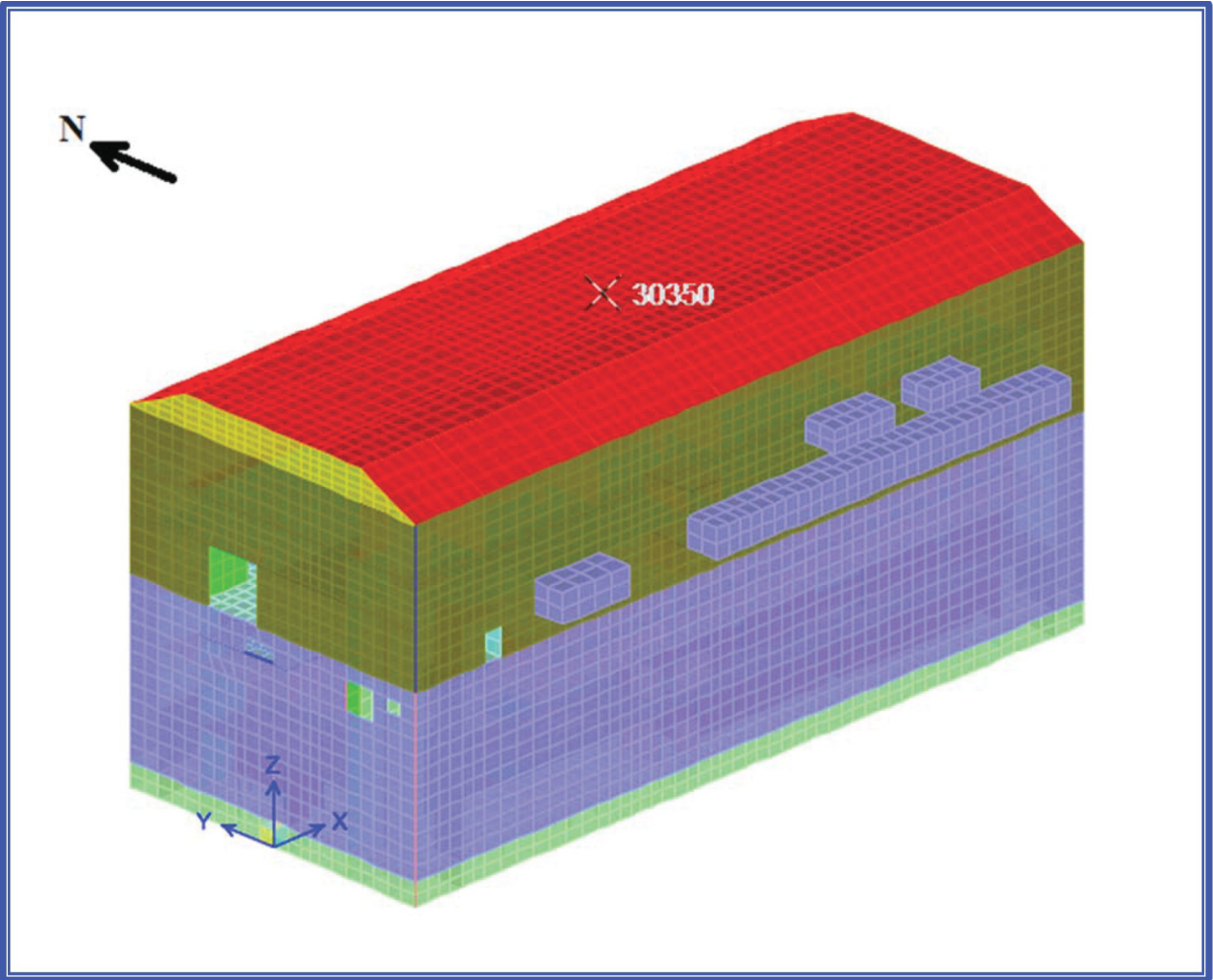


Figure 1-4. Node 30350, Roof Slab between Grid Lines RX-4 and RX-5 (Center).

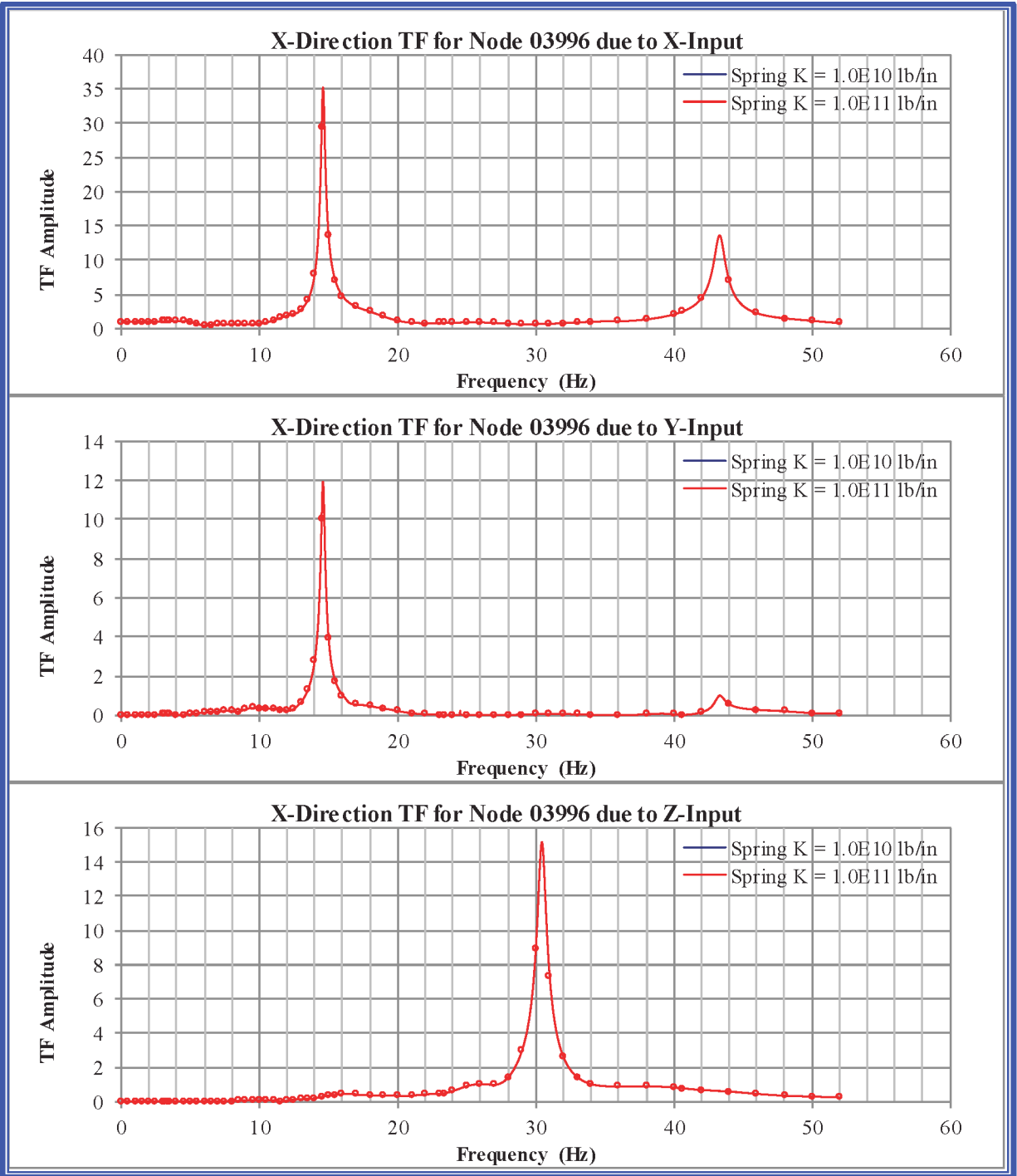


Figure 1-5. Cracked RXB X Acceleration Transfer Function Amplitude Comparison at Node 3996, Northwest Corner on Top of Basemat, for Soil Type 7.

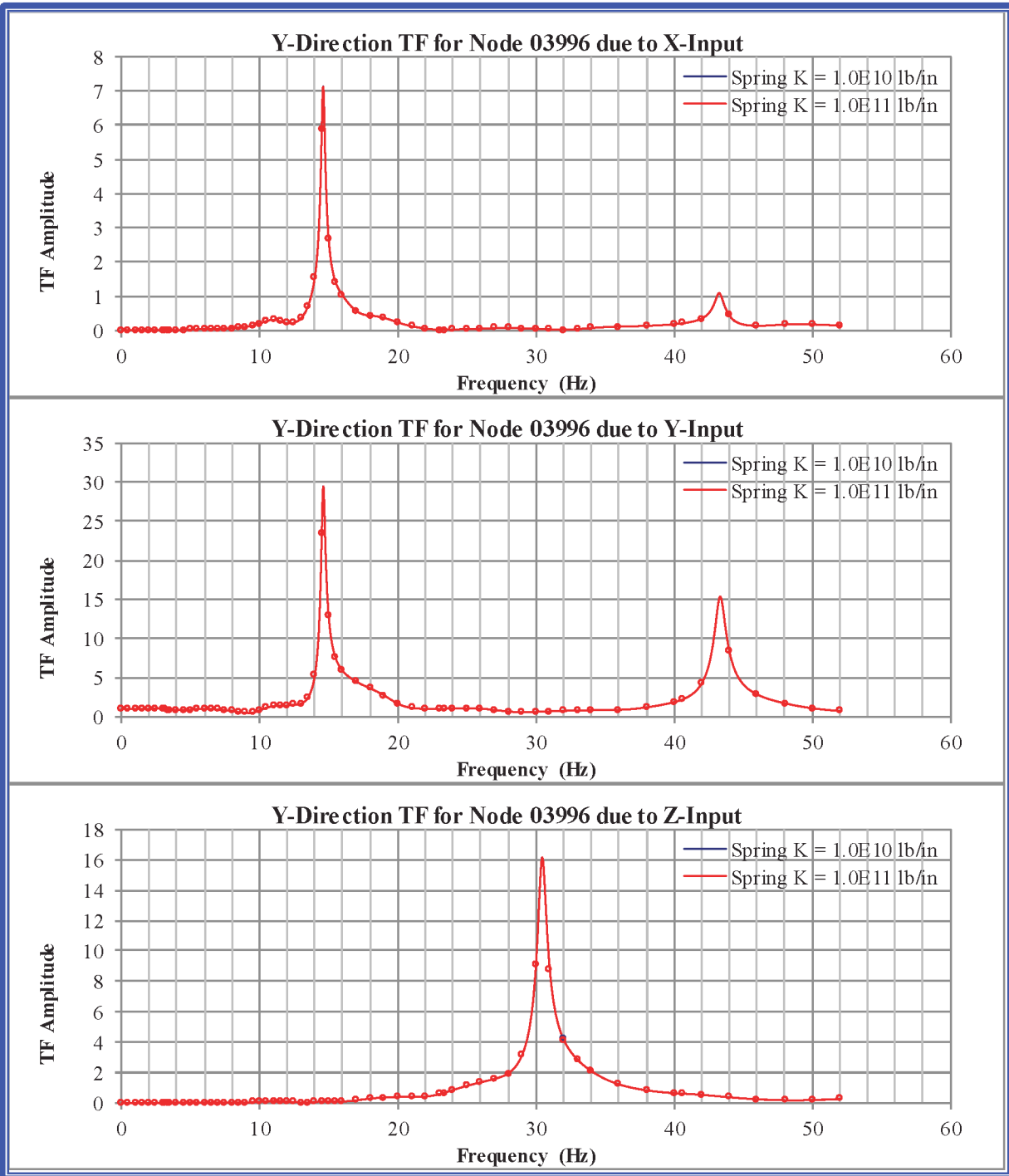


Figure 1-6. Cracked RXB Y Acceleration Transfer Function Amplitude Comparison at Node 3996, Northwest Corner on Top of Basemat, for Soil Type 7.

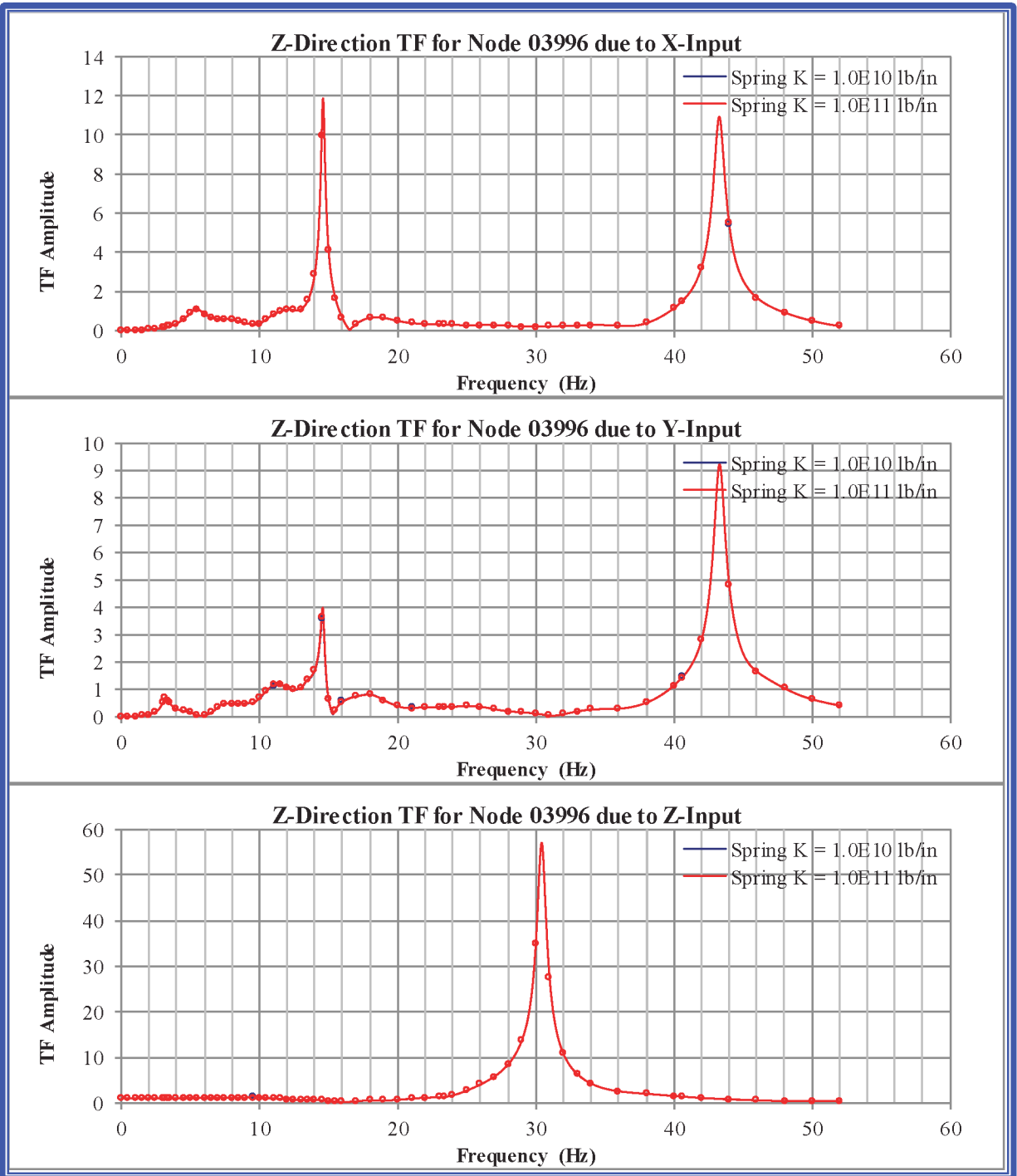


Figure 1-7. Cracked RXB Z Acceleration Transfer Function Amplitude Comparison at Node 3996, Northwest Corner on Top of Basemat, for Soil Type 7.

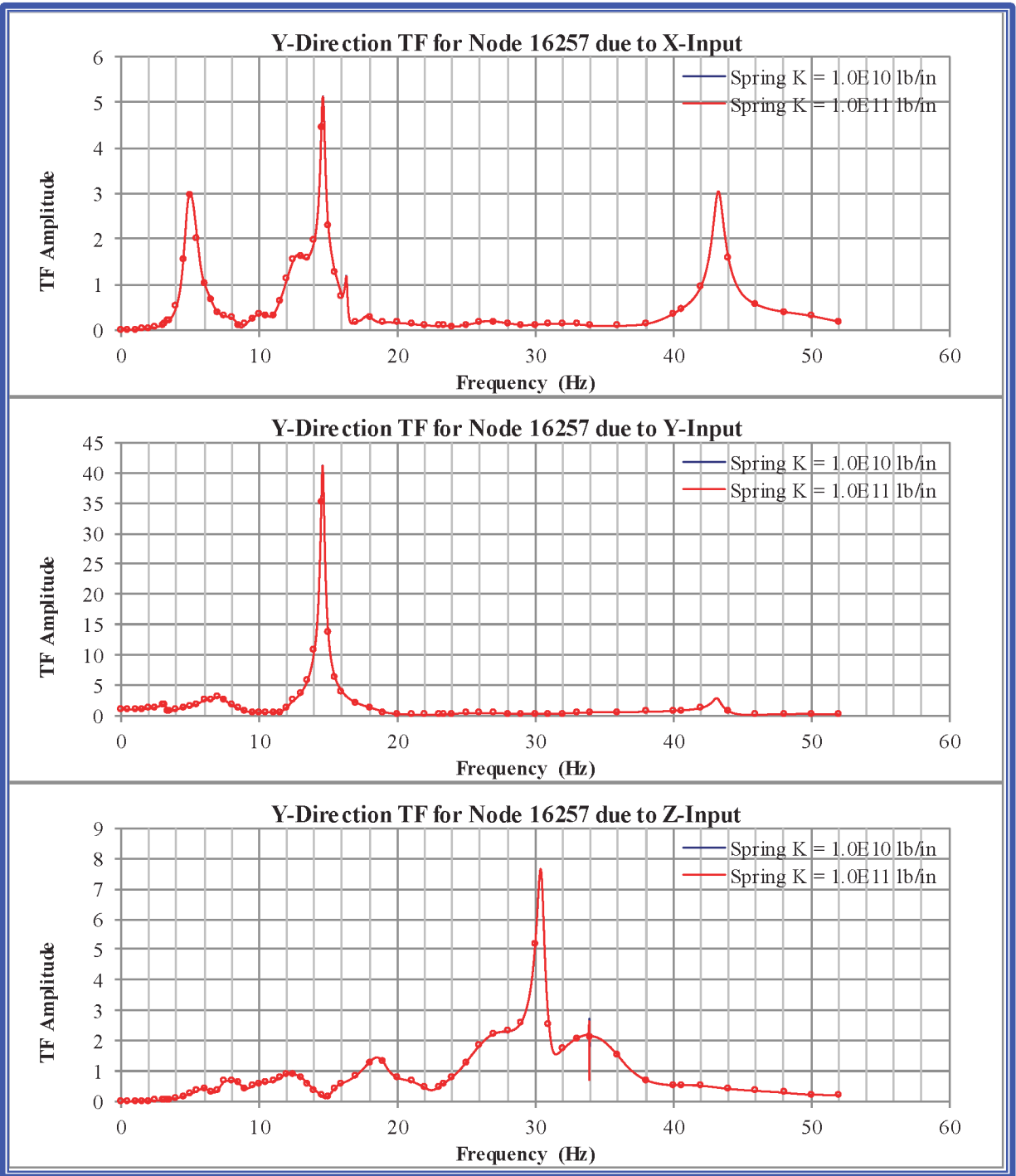


Figure 1-8. Cracked RXB Y Acceleration Transfer Function Amplitude Comparison at Node 16257, RXM 1 at West Lug Support Location, for Soil Type 7.

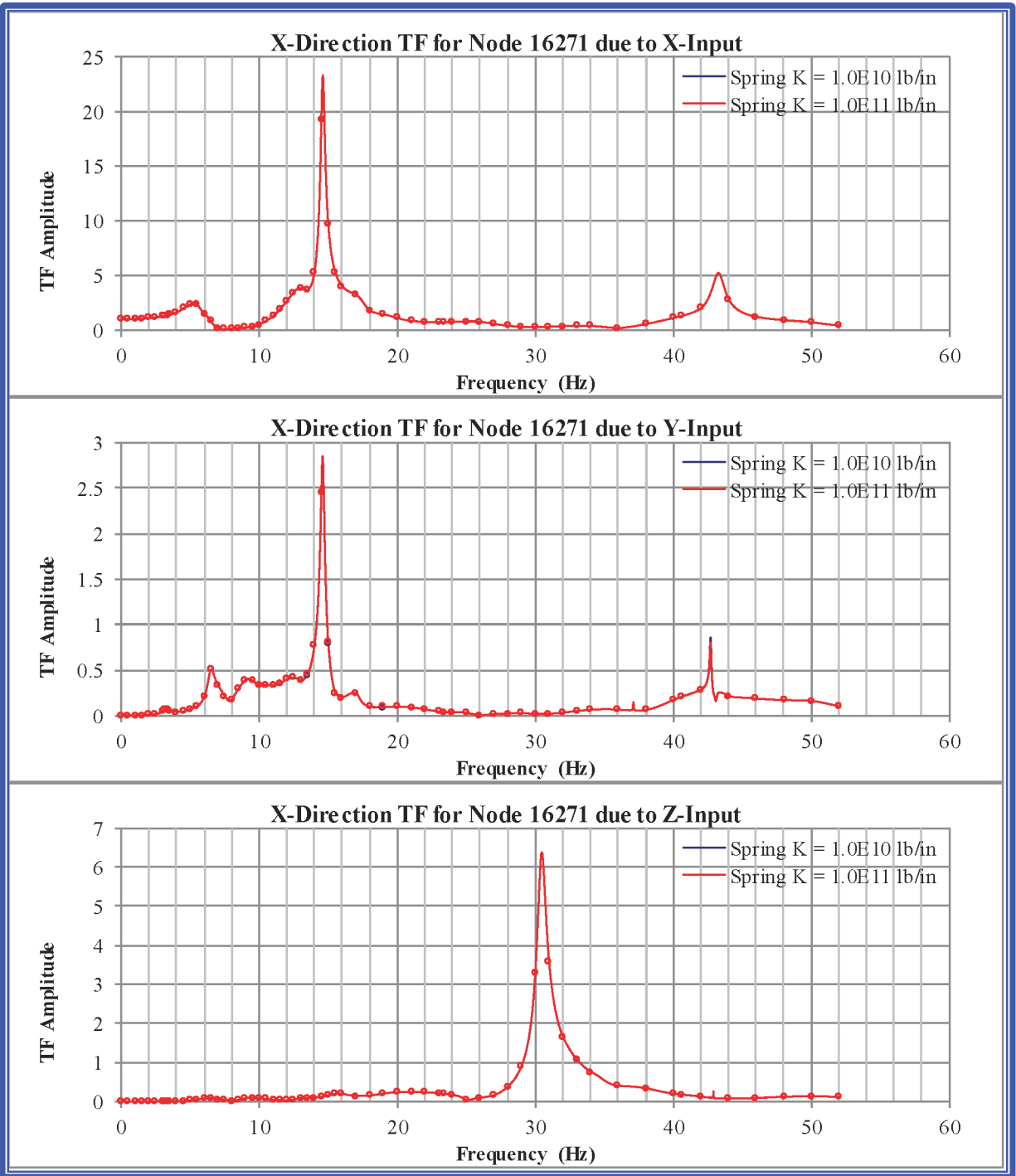


Figure 1-9. Cracked RXB X Acceleration Transfer Function Amplitude Comparison at Node 16271, RXM 1 at North Lug Support Location, for Soil Type 7.

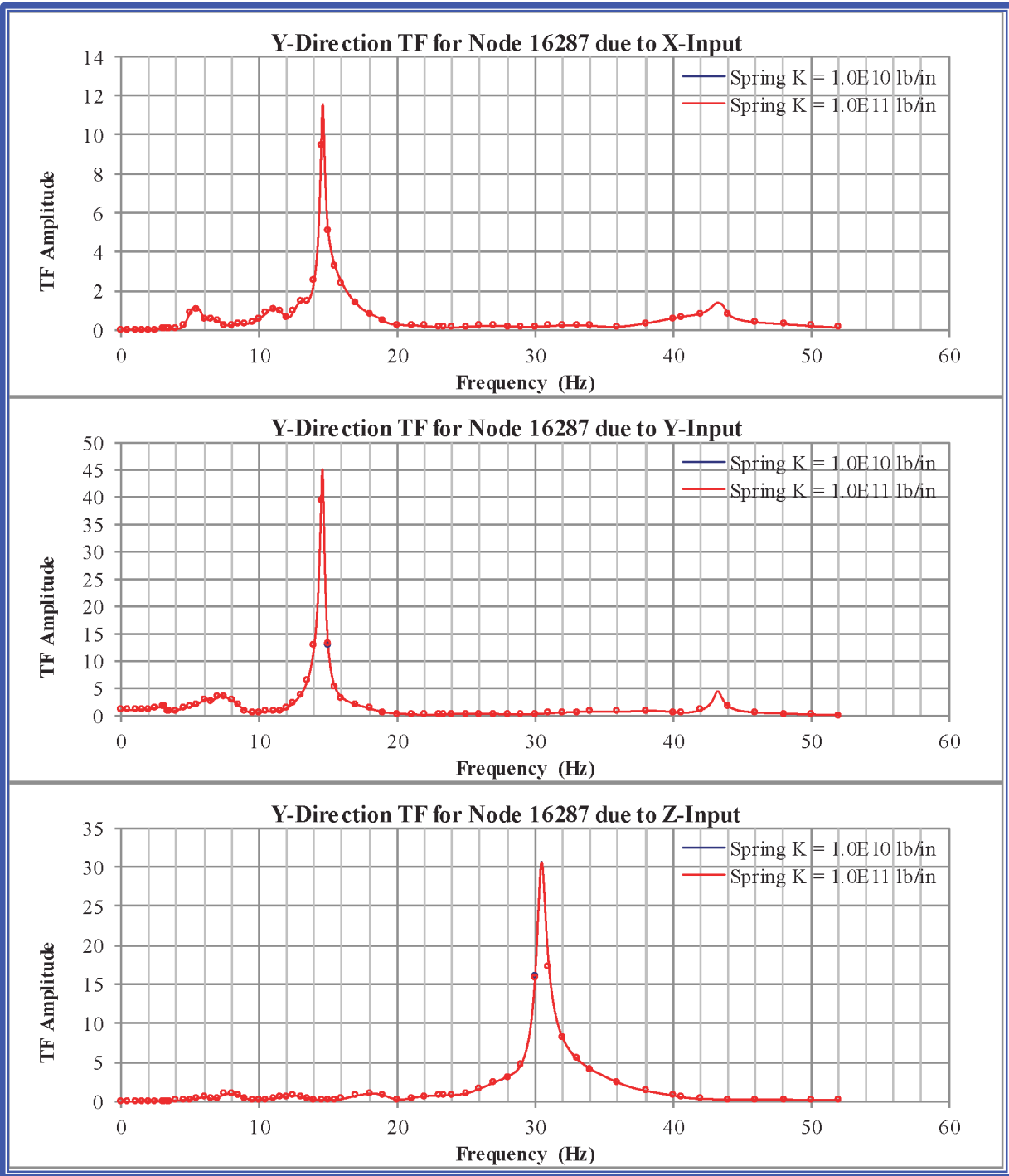


Figure 1-10. Cracked RXB Y Acceleration Transfer Function Amplitude Comparison at Node 16287, RXM 1 at East Lug Support Location, for Soil Type 7.

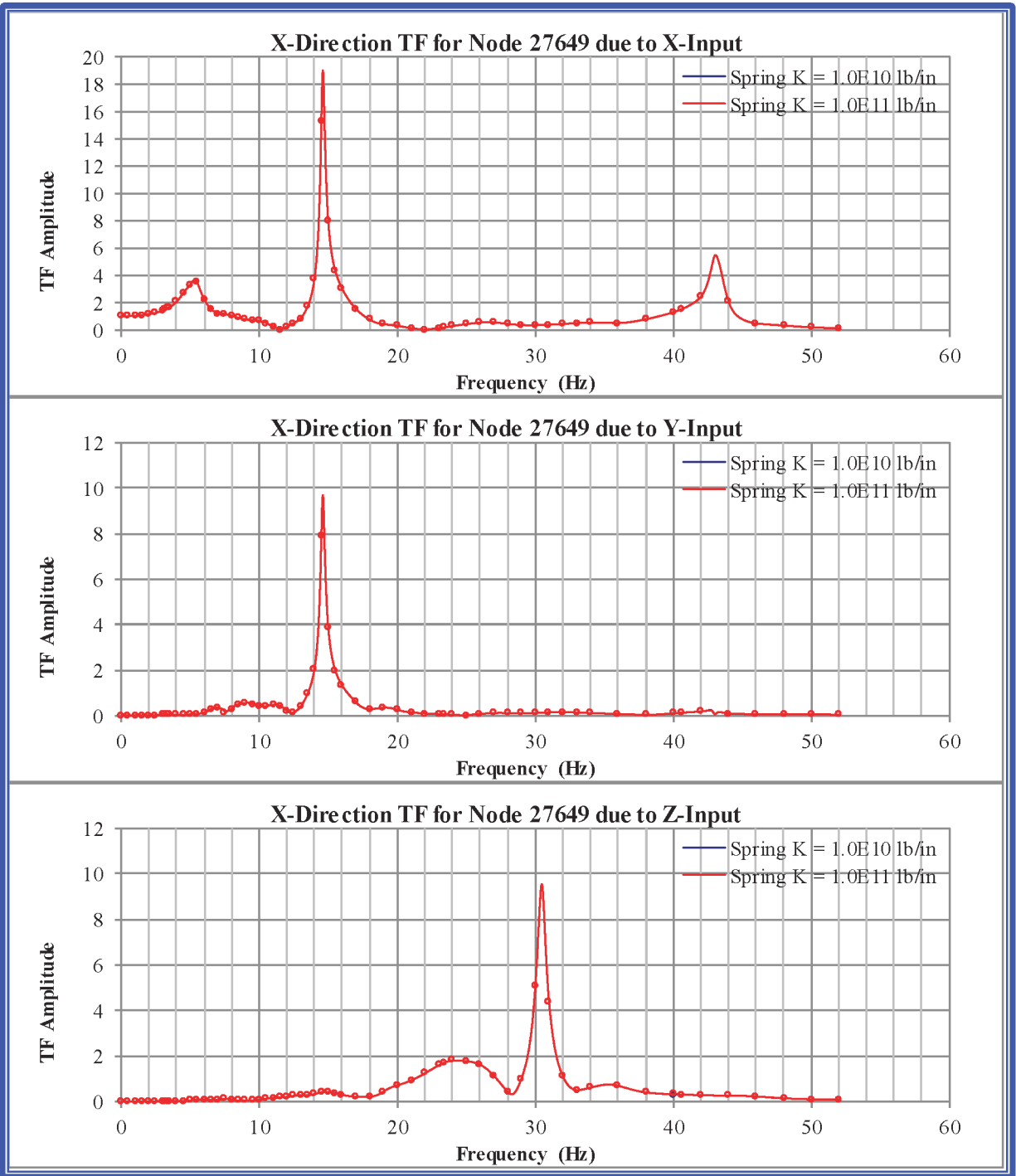


Figure 1-11. Cracked RXB X Acceleration Transfer Function Amplitude Comparison at Node 27649, Crane Rail Slab at Grid Line RX-4 at El. 145'-6", for Soil Type 7.

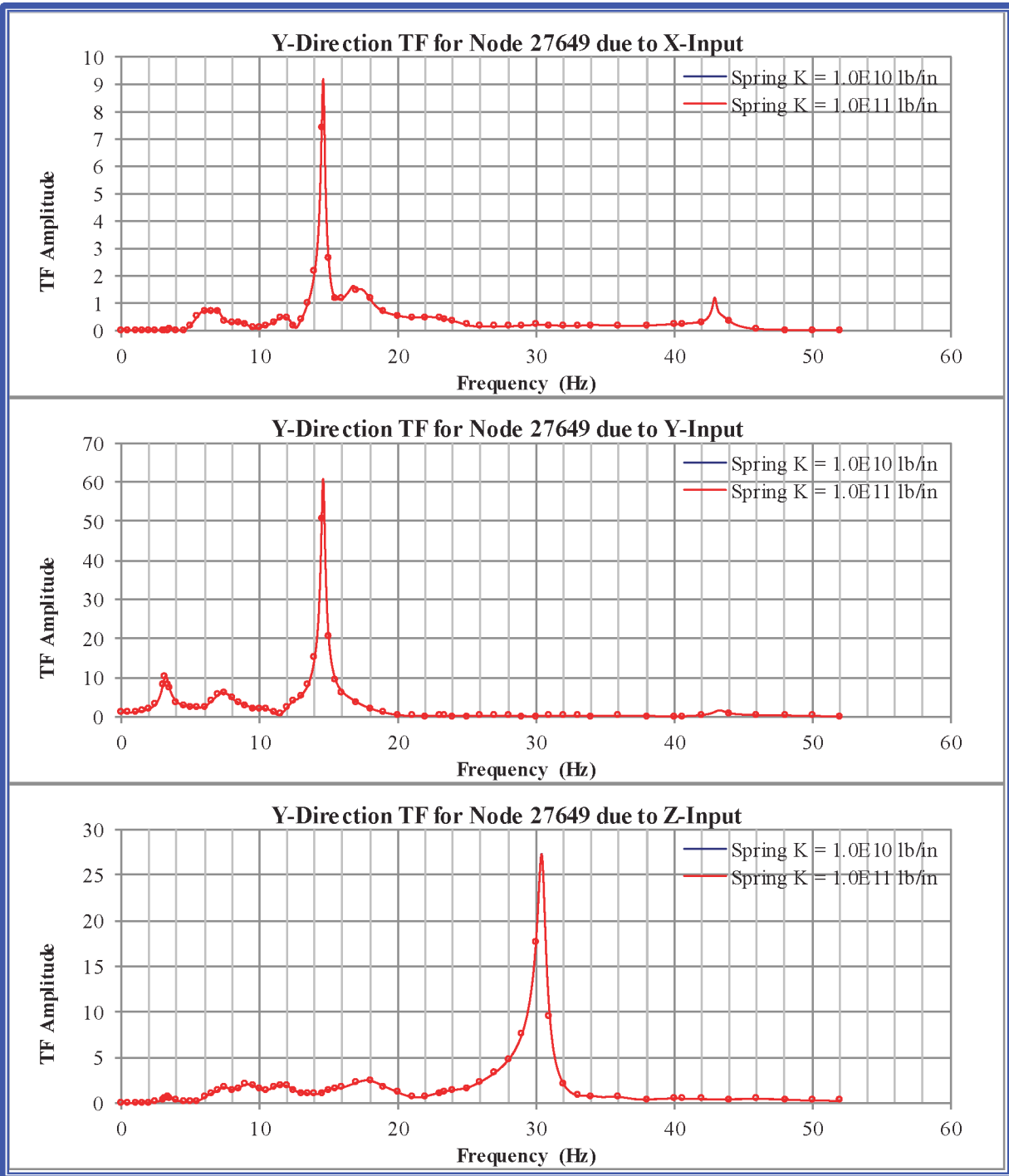


Figure 1-12. Cracked RXB Y Acceleration Transfer Function Amplitude Comparison at Node 27649, Crane Rail Slab at Grid Line RX-4 at El. 145'-6", for Soil Type 7.

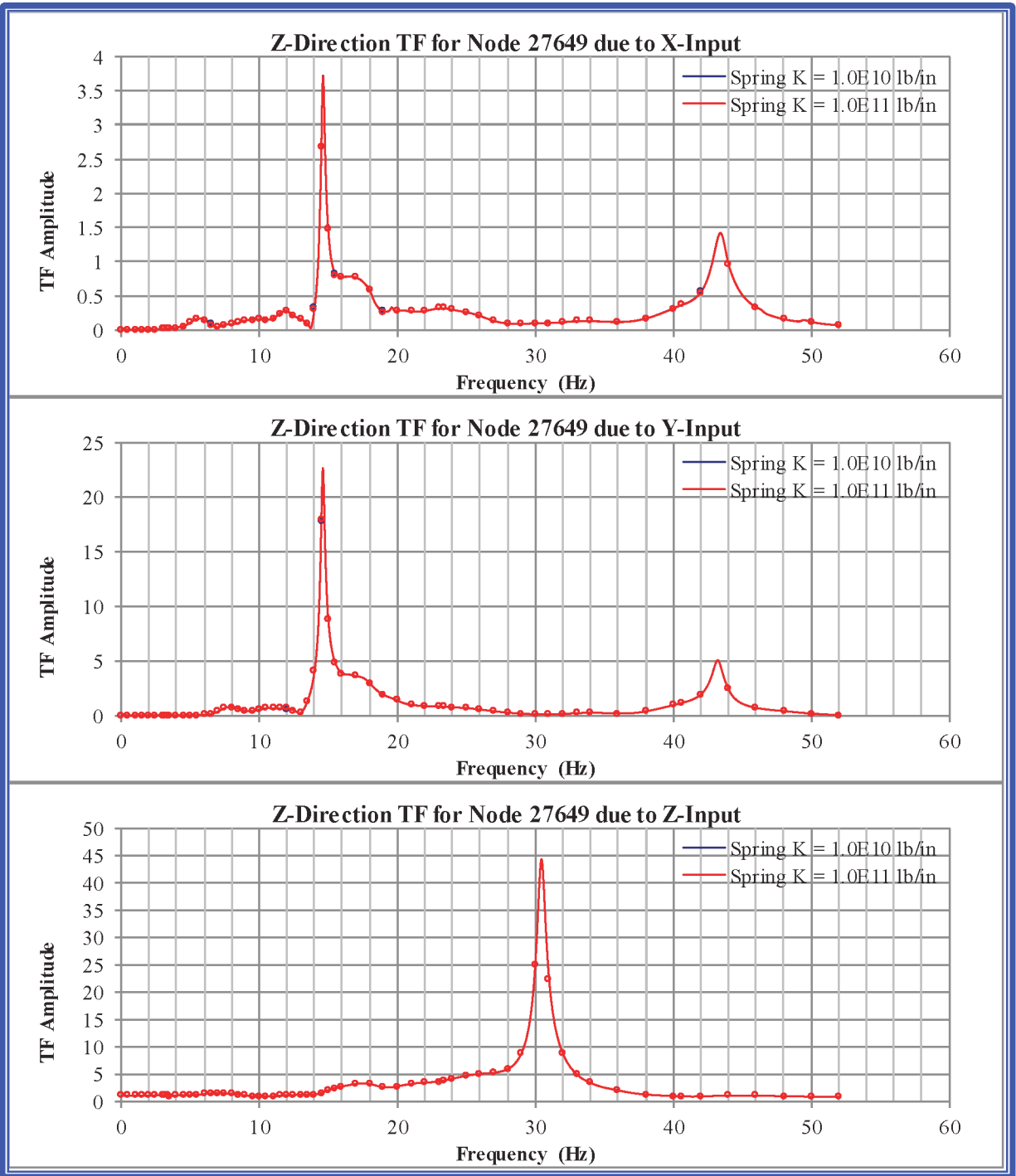


Figure 1-13. Cracked RXB Z Acceleration Transfer Function Amplitude Comparison at Node 27649, Crane Rail Slab at Grid Line RX-4 at El. 145'-6", for Soil Type 7.

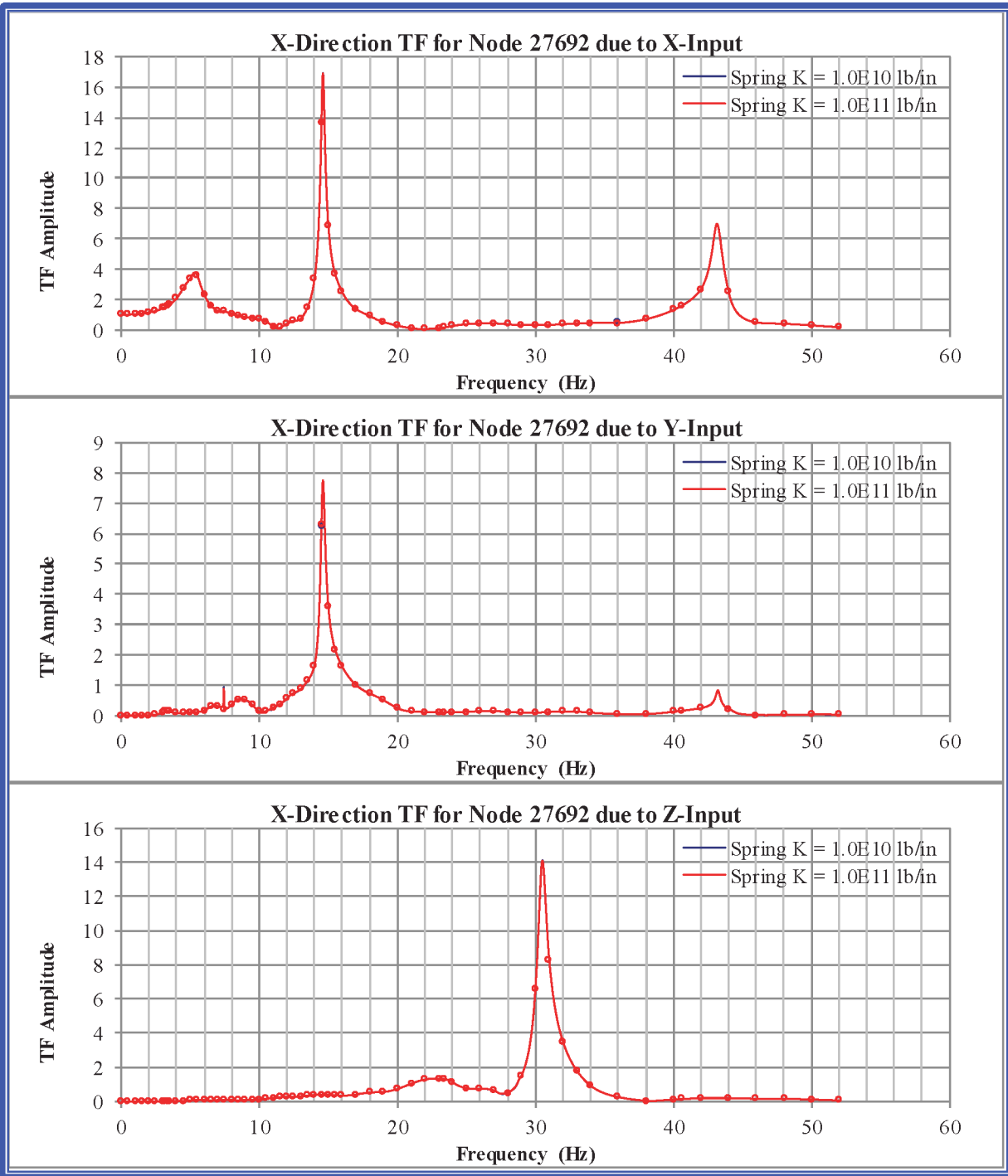


Figure 1-14. Cracked RXB X Acceleration Transfer Function Amplitude Comparison at Node 27692, Crane Rail Slab between Grid Lines RX-4 and RX-5 at El. 145'-6", for Soil Type 7.

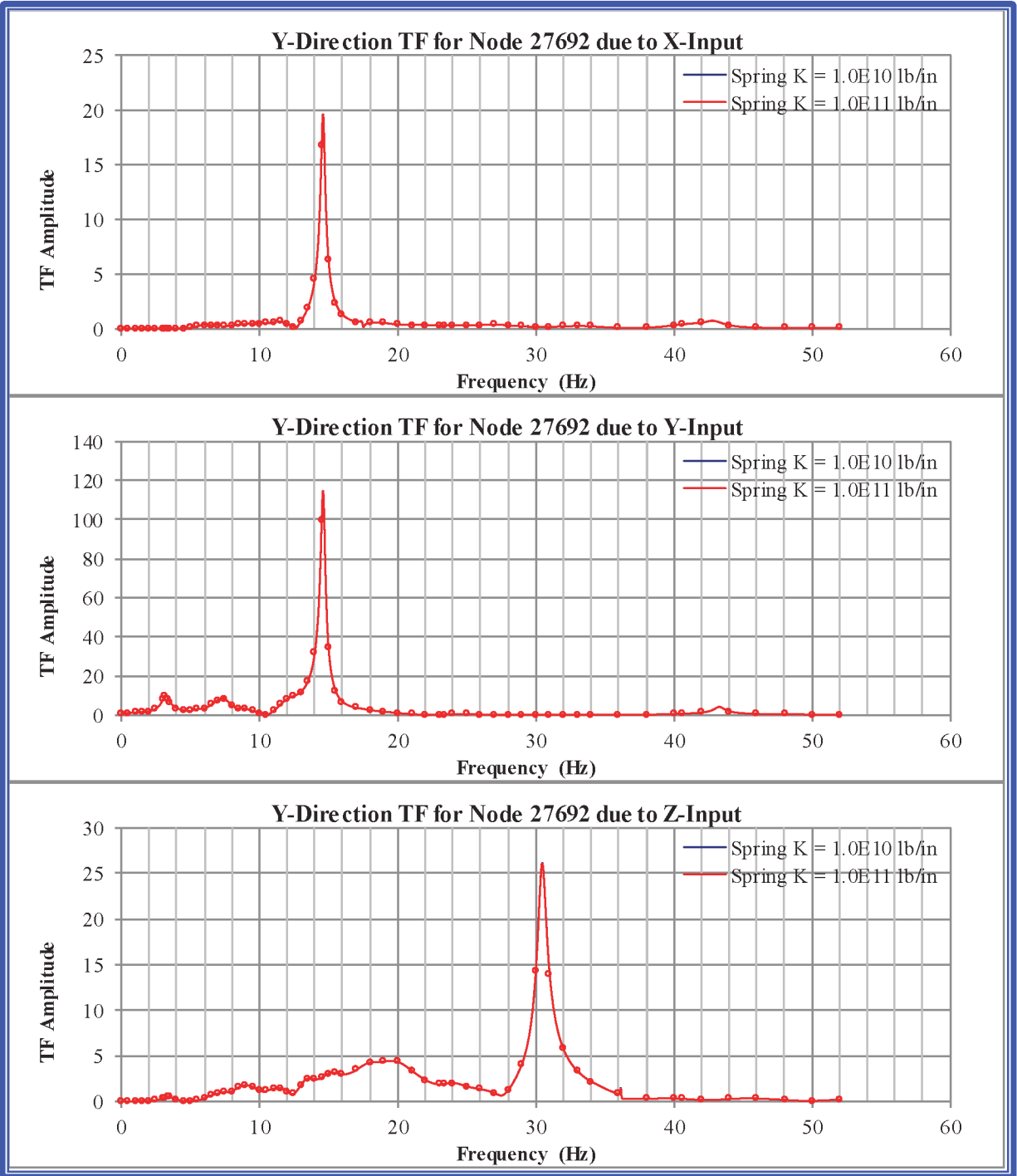


Figure 1-15. Cracked RXB Y Acceleration Transfer Function Amplitude Comparison at Node 27692, Crane Rail Slab between Grid Lines RX-4 and RX-5 at El. 145'-6", for Soil Type 7.

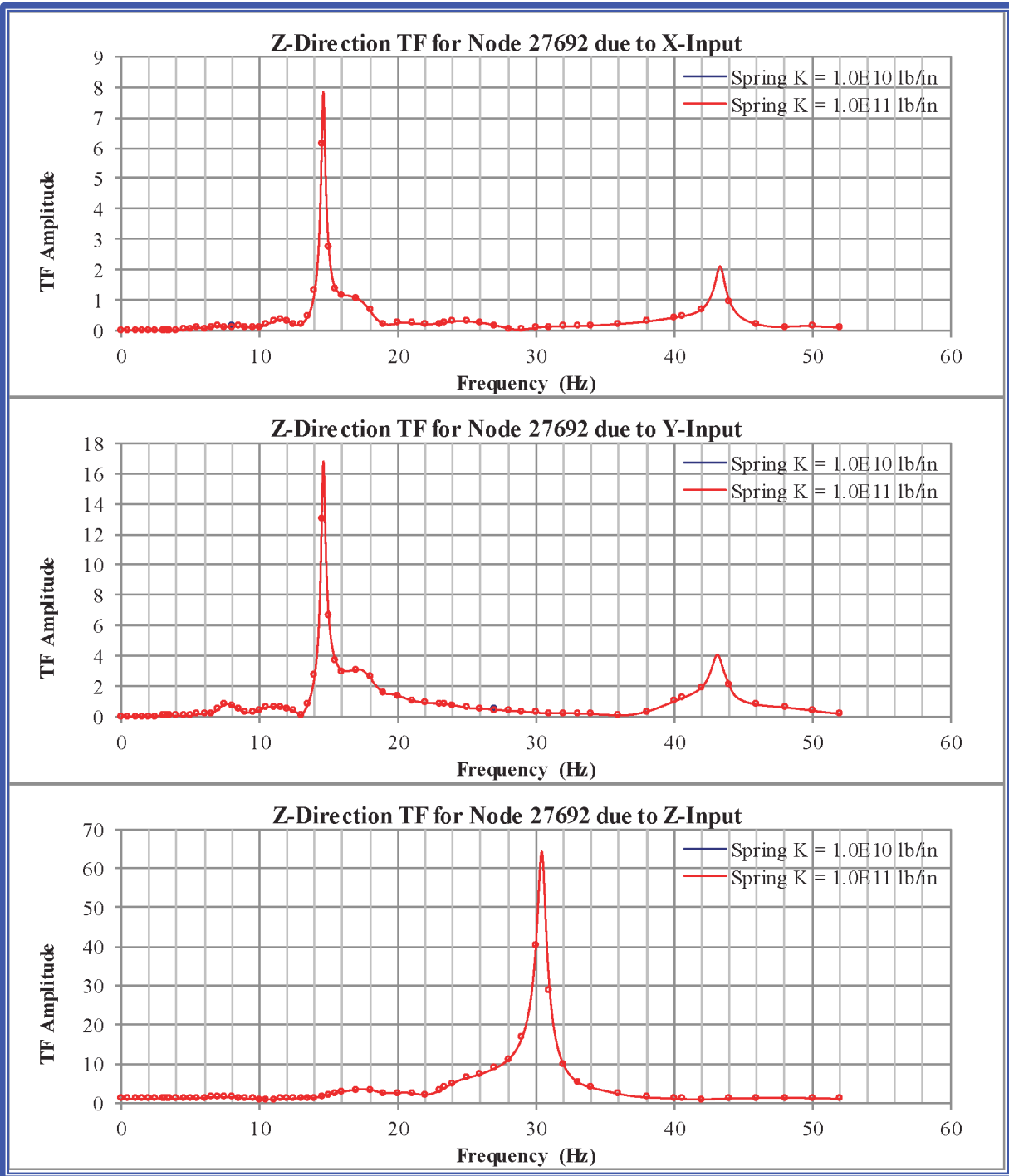


Figure 1-16. Cracked RXB Z Acceleration Transfer Function Amplitude Comparison at Node 27692, Crane Rail Slab between Grid Lines RX-4 and RX-5 at El. 145'-6", for Soil Type 7.

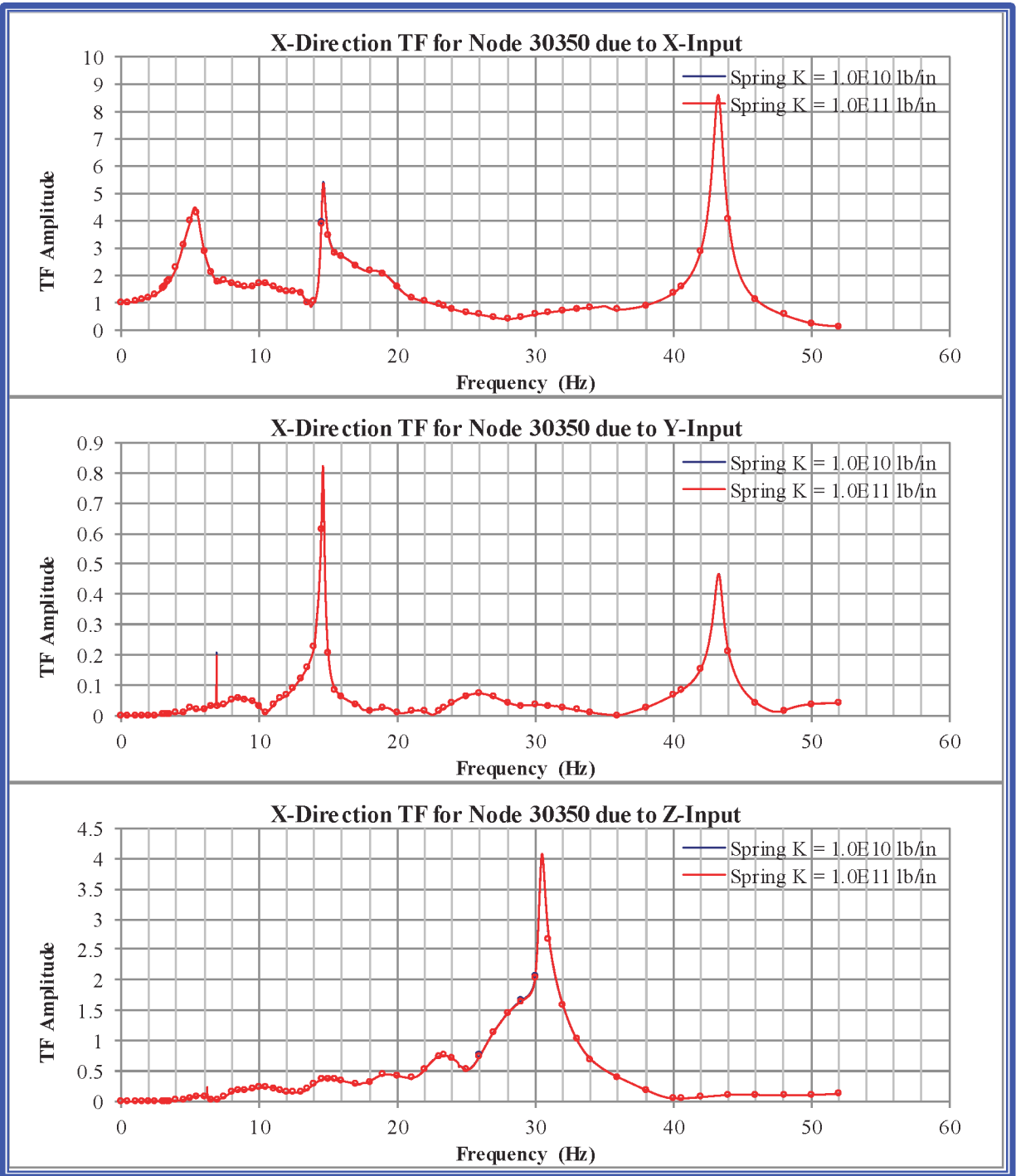


Figure 1-17. Cracked RXB X Acceleration Transfer Function Amplitude Comparison at Node 30350, Roof Slab between Grid Lines RX-4 and RX-5, for Soil Type 7.

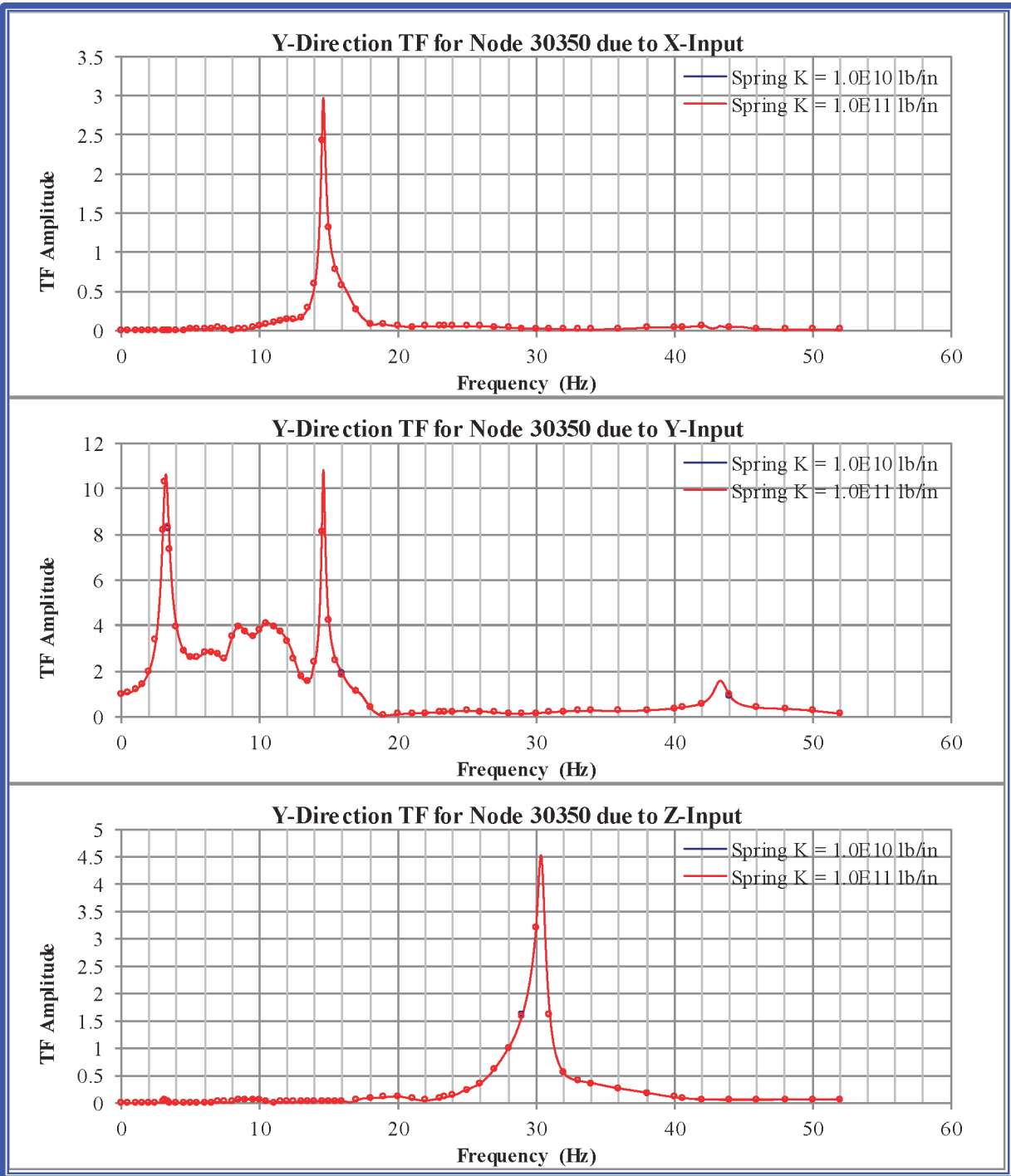


Figure 1-18. Cracked RXB Y Acceleration Transfer Function Amplitude Comparison at Node 30350, Roof Slab between Grid Lines RX-4 and RX-5, for Soil Type 7.

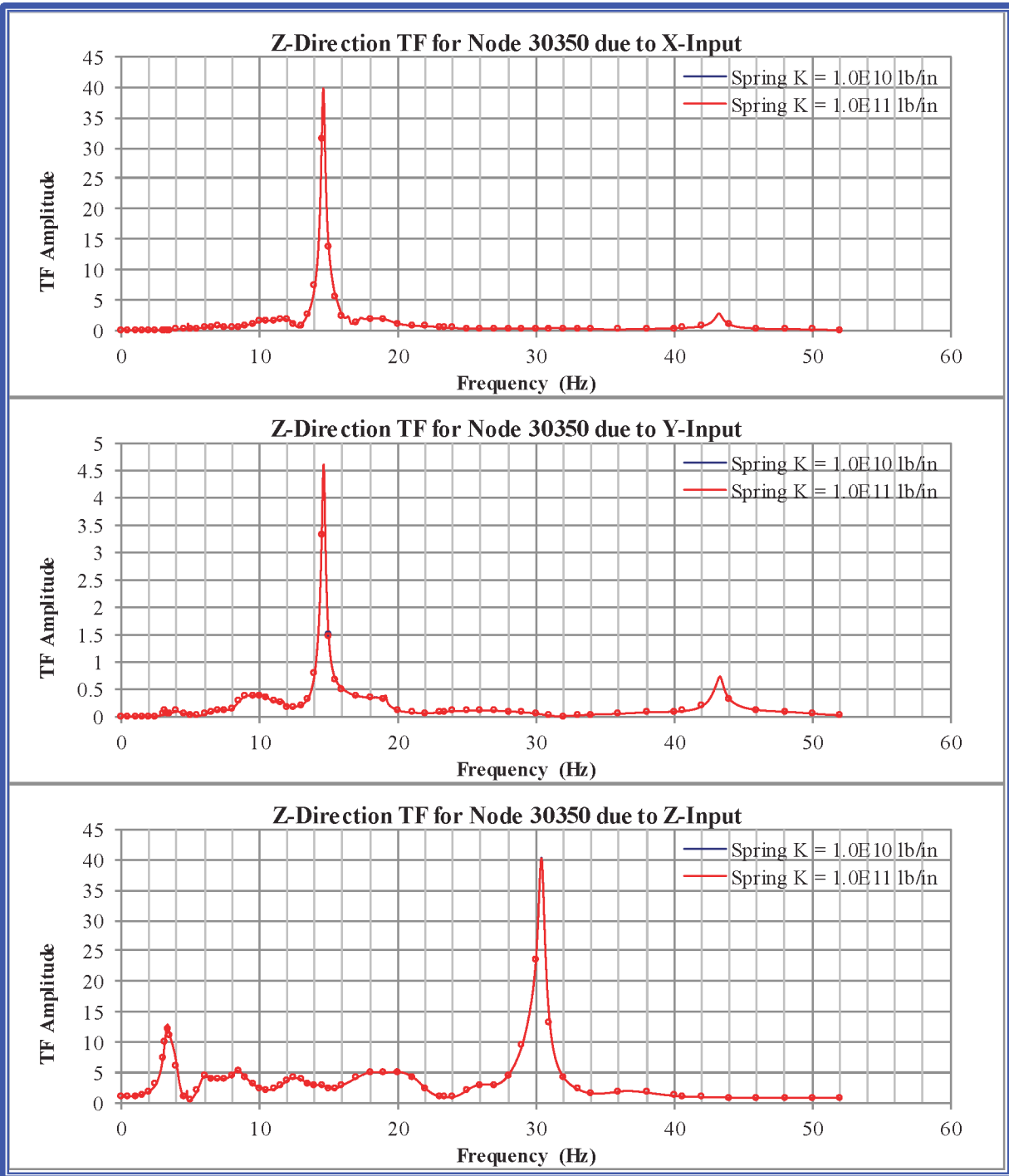


Figure 1-19. Cracked RXB Z Acceleration Transfer Function Amplitude Comparison at Node 30350, Roof Slab between Grid Lines RX-4 and RX-5, for Soil Type 7.

1.2 ISRS Comparison

In this section, ISRS comparisons are provided at the same locations listed in Table 1-1 and shown in Figure 1-1 through Figure 1-4. As before, ISRS comparisons at the lugs are only presented in the direction in which the lugs are restrained, that is, in the NS direction for the west and east lugs, and in the EW direction for the north and south lugs. The co-directional responses due to the three input directions have been combined using the square-root-of-the-sum-of-the-squares (SRSS) method.

The cracked concrete model with 7% concrete damping was used to generate these results. Results are presented for the Capitola input case.

The ISRS comparisons are shown in Figure 1-20 through Figure 1-34. There are no discernible differences in the ISRS generated with spring $K = 10^{10}$ lb/in and spring $K = 10^{11}$ lb/in.

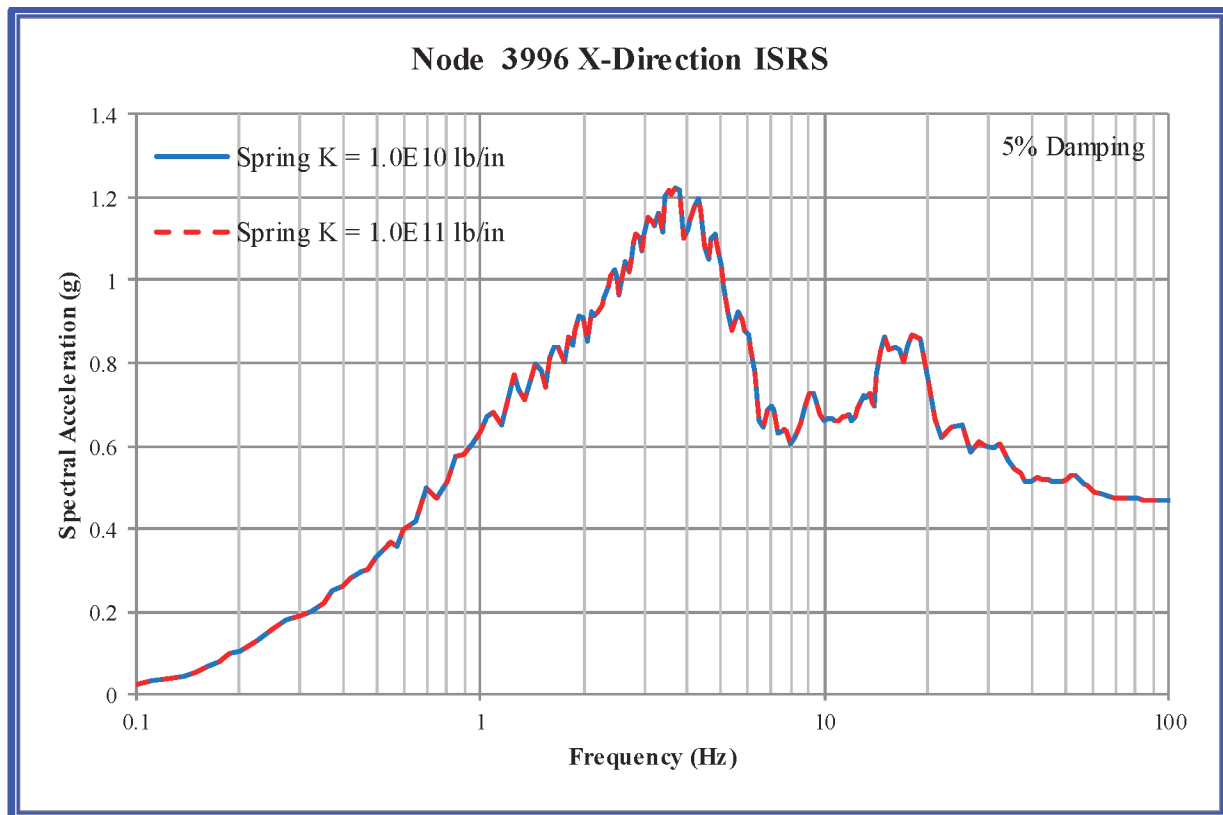


Figure 1-20. RXB - East-West (X) ISRS, Node 3996, Northwest Corner on Top of Basemat, Capitola Input.

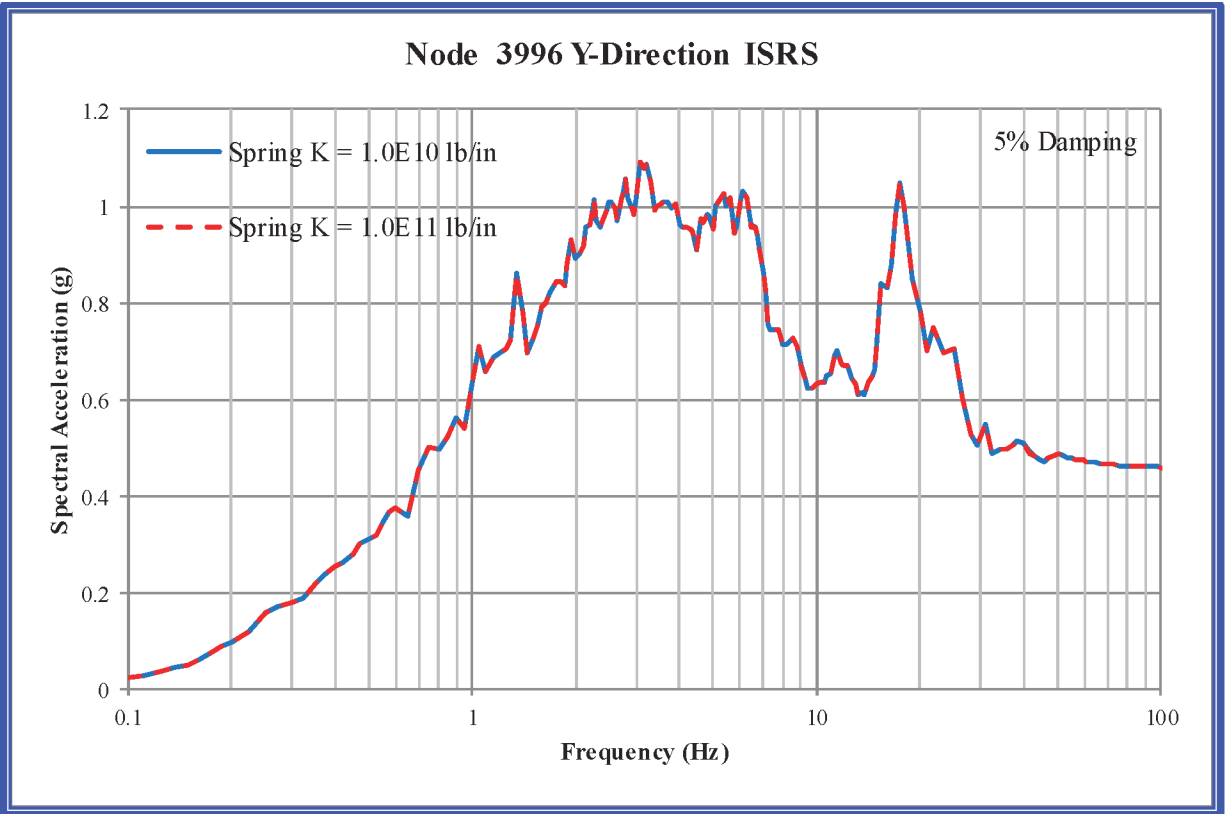


Figure 1-21. RXB - North-South (Y) ISRS, Node 3996, Northwest Corner on Top of Basemat, Capitola Input.

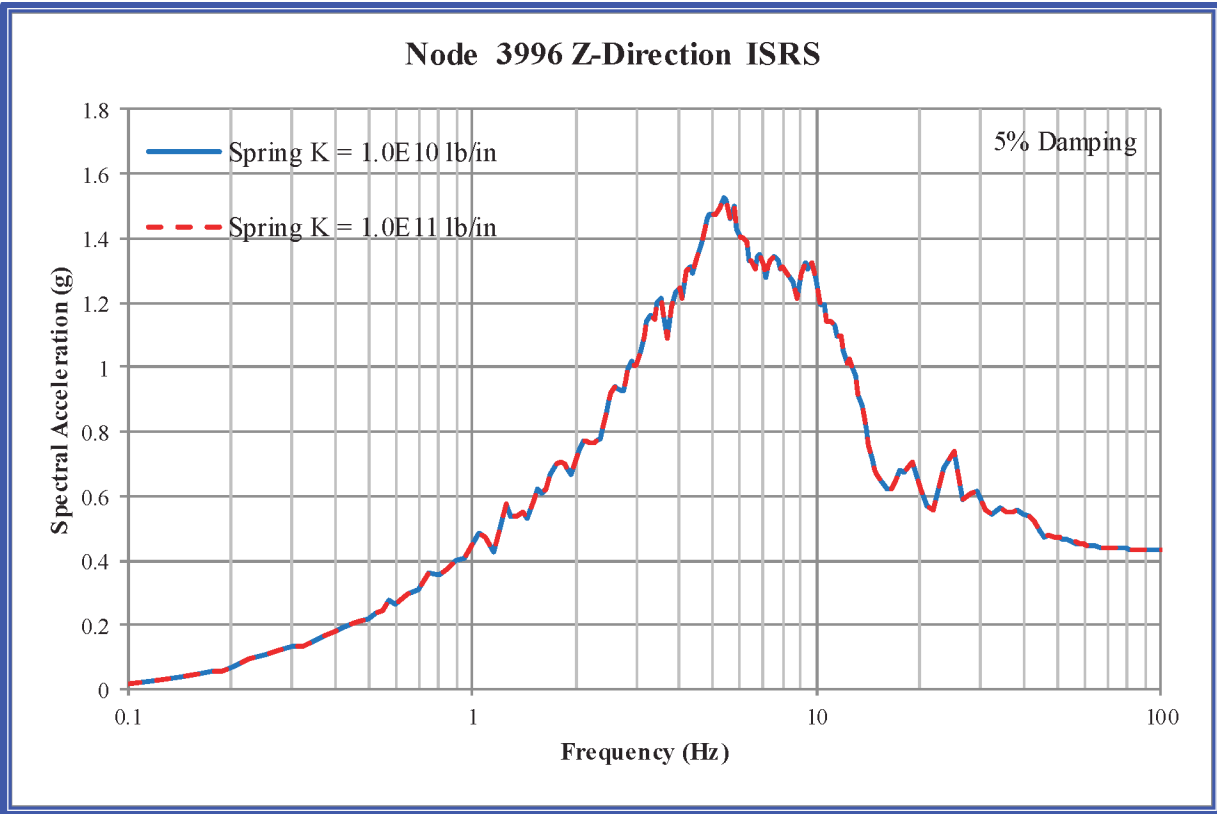


Figure 1-22. RXB - Vertical (Z) ISRS, Node 3996, Northwest Corner on Top of Basemat, Capitola Input.

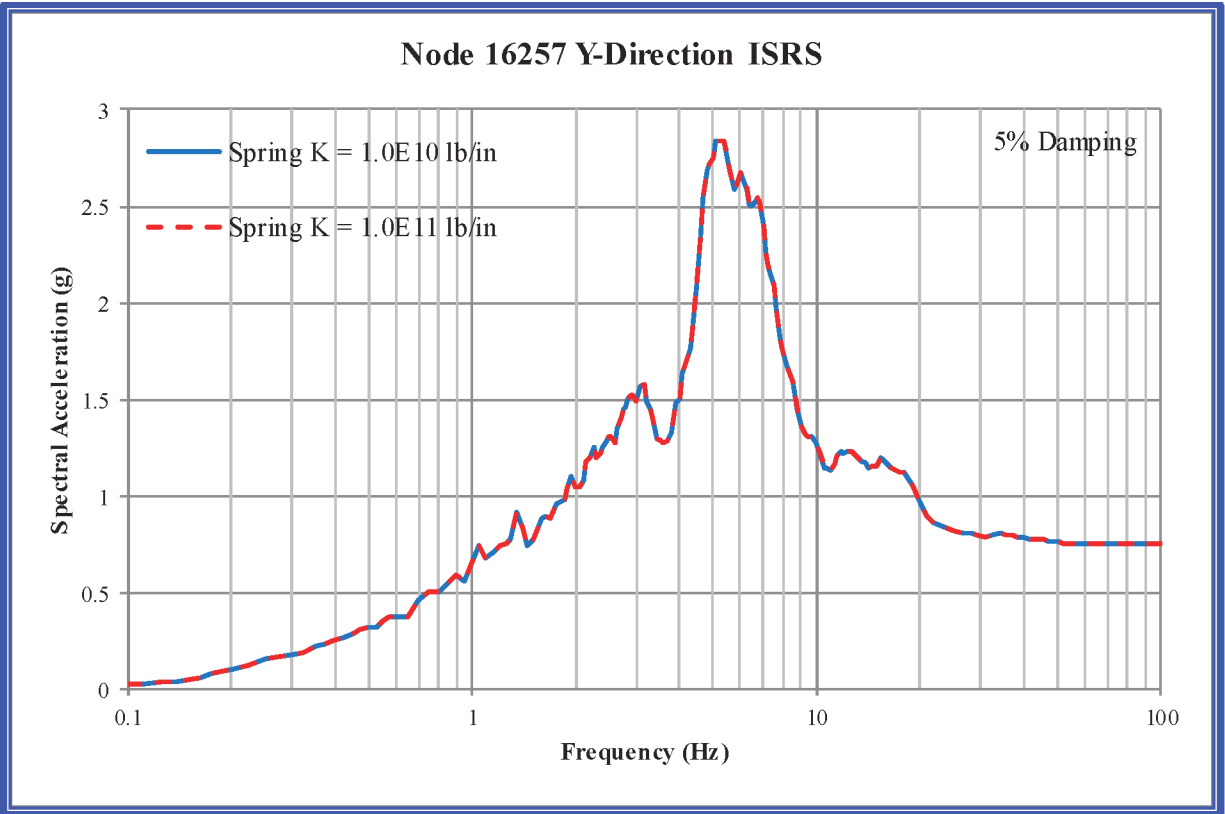


Figure 1-23. RXB - North-South (Y) ISRS, Node 16257, RXM 1 at West Lug Support Location, Capitola Input.

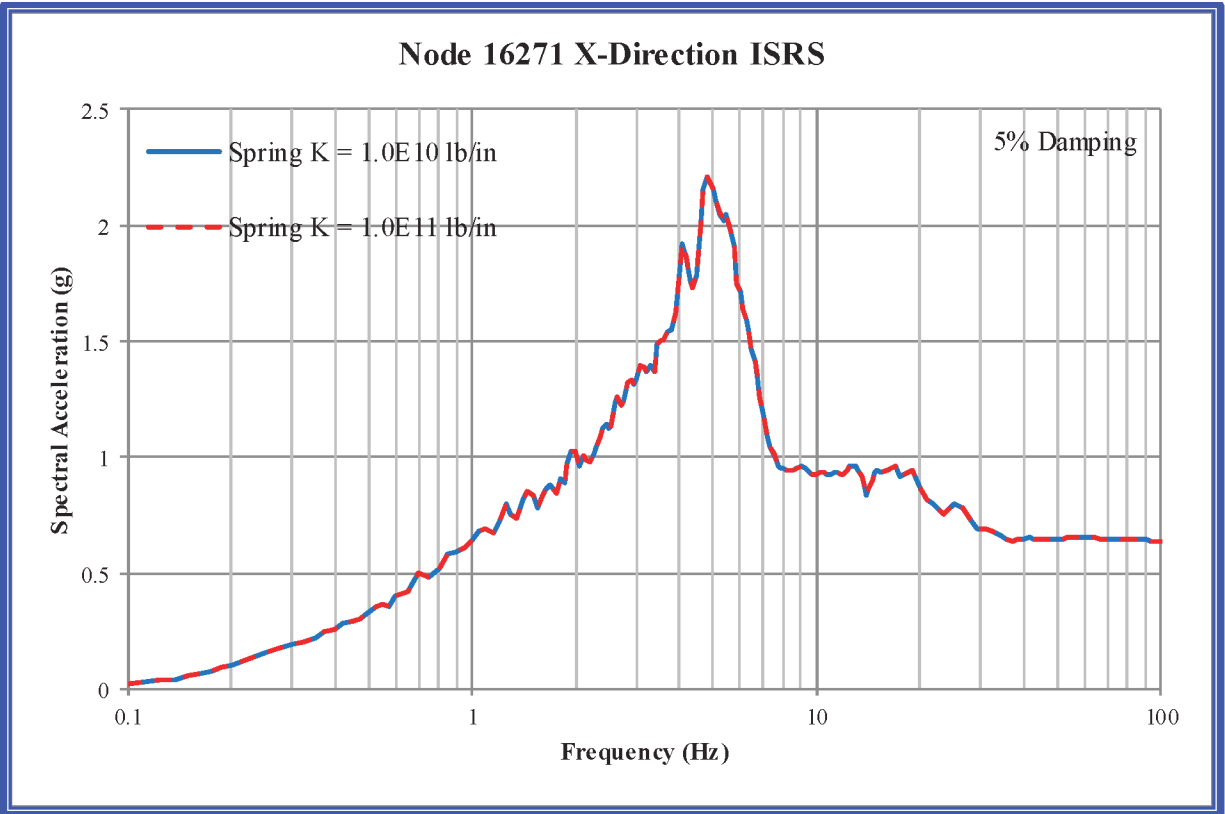


Figure 1-24. RXB - East-West (X) ISRS, Node 16271, RXM 1 at North Lug Support Location, Capitola Input.

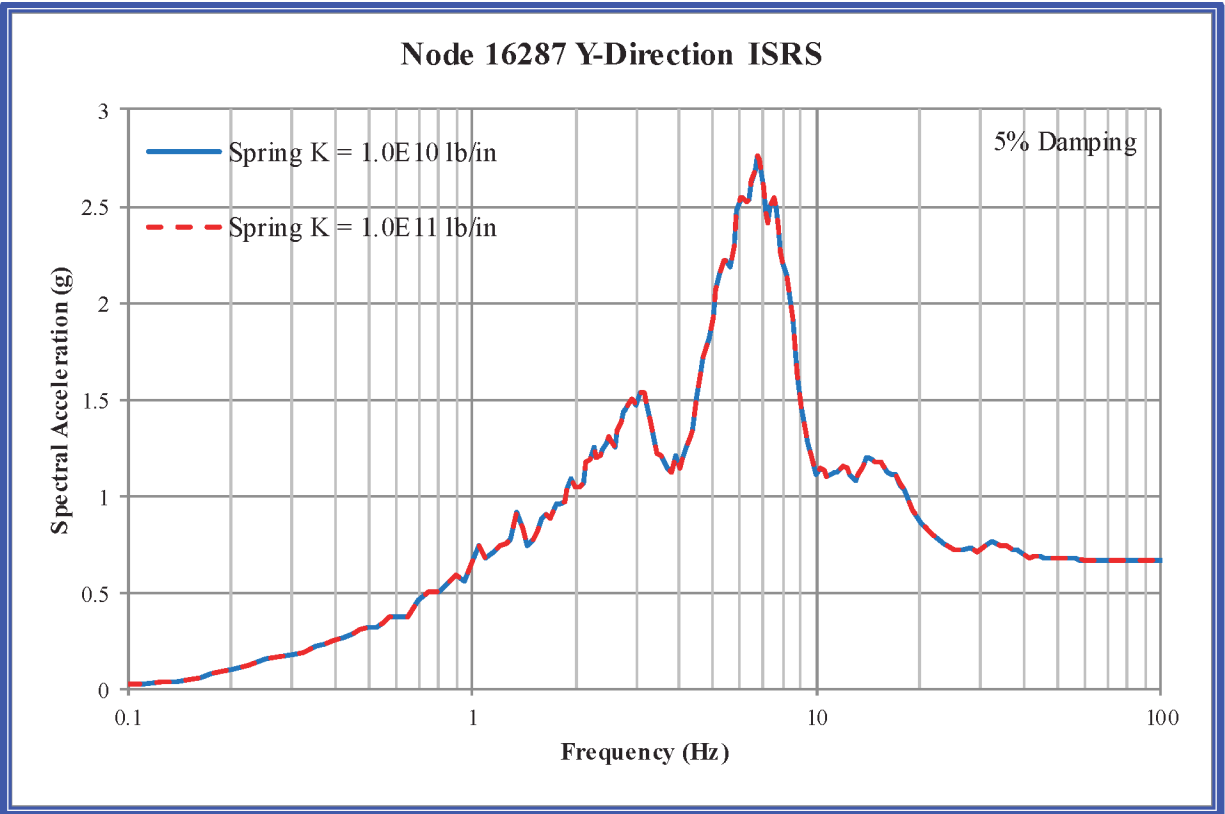


Figure 1-25. RXB - North-South (Y) ISRS, Node 16287, RXM 1 at East Lug Support Location, Capitola Input.

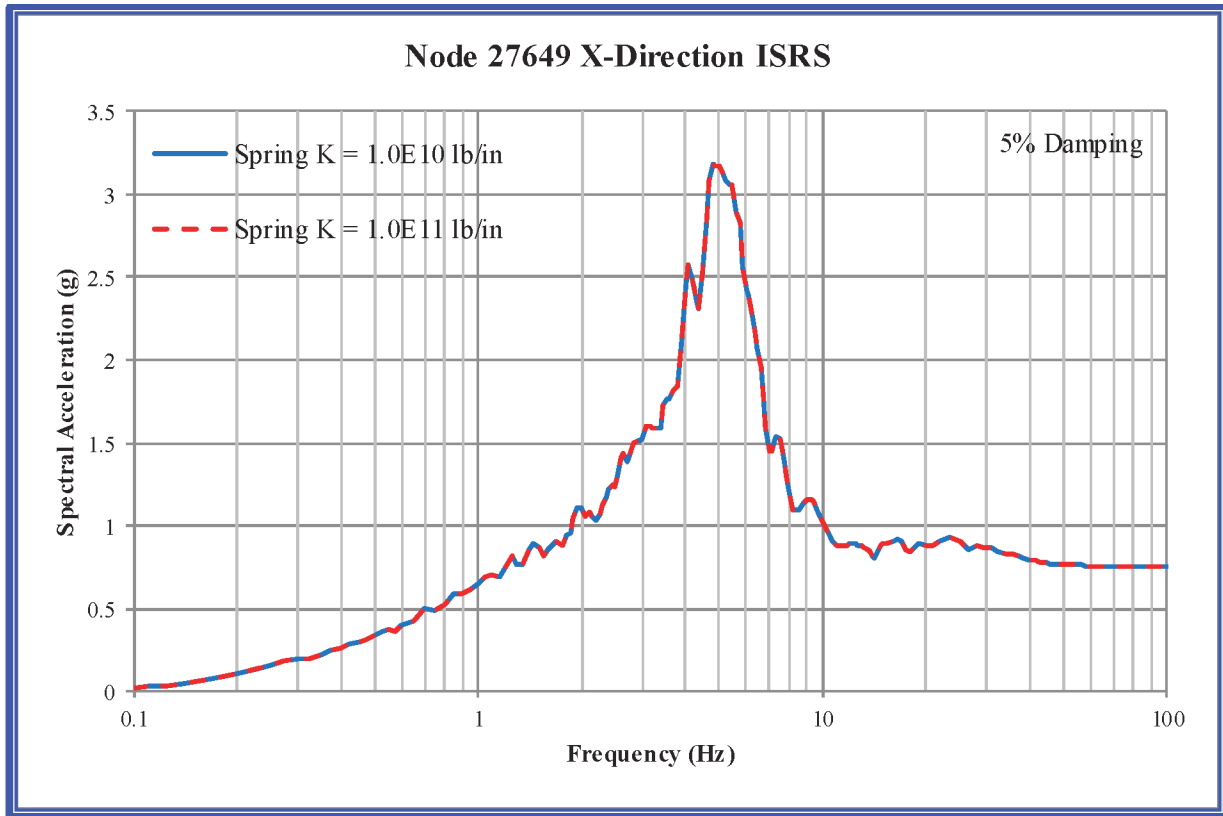


Figure 1-26. RXB - East-West (X) ISRS, Node 27649, Crane Rail Slab at Grid Line RX-4 at El. 145'-6", Capitola Input.

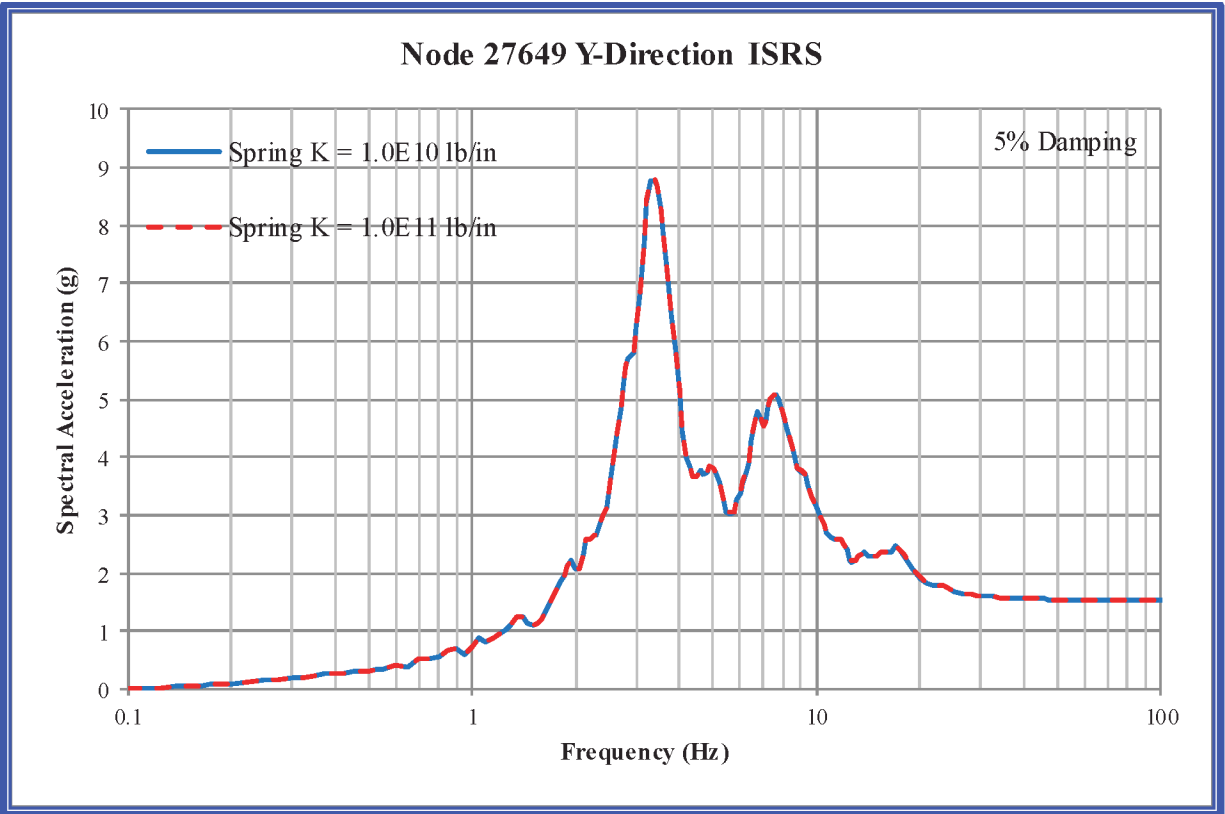


Figure 1-27. RXB - North-South (Y) ISRS, Node 27649, Crane Rail Slab at Grid Line RX-4 at El. 145'-6", Capitola Input.

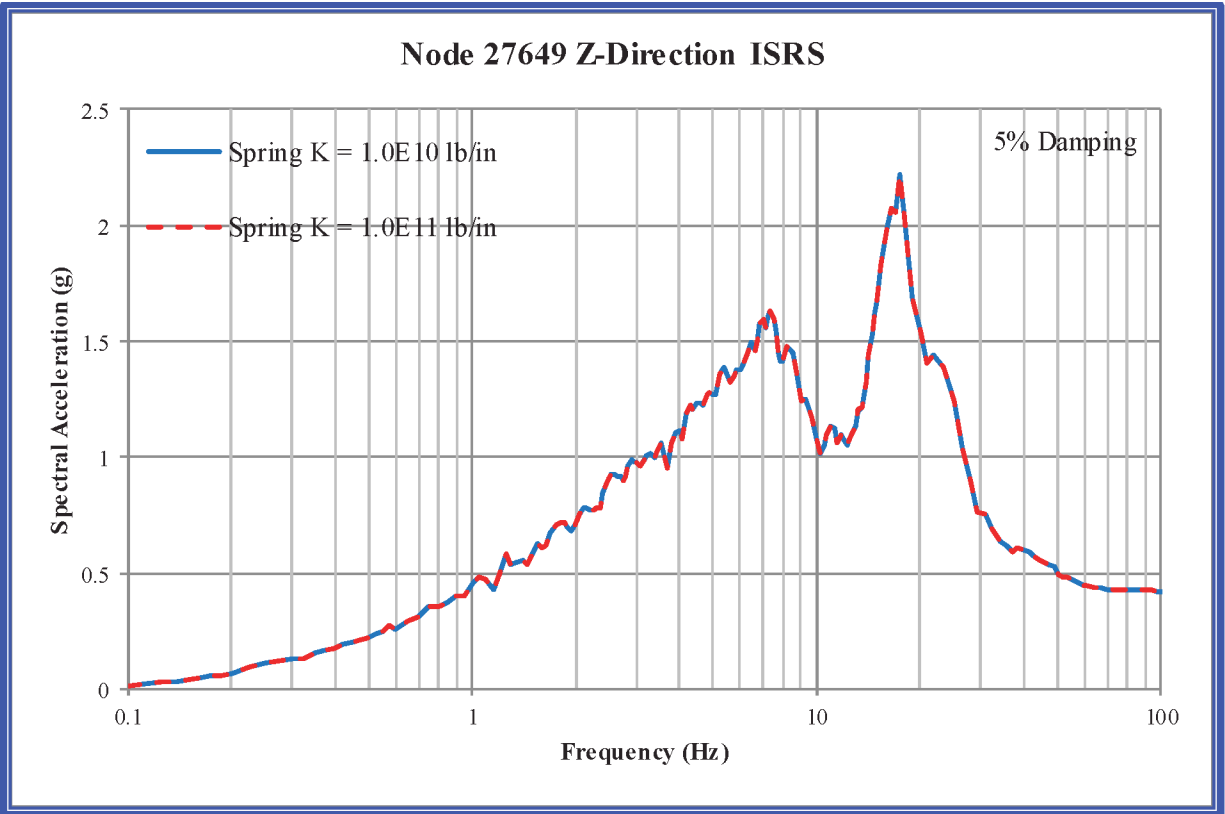


Figure 1-28. RXB - Vertical (Z) ISRS, Node 27649, Crane Rail Slab at Grid Line RX-4 at El. 145'-6", Capitola Input.

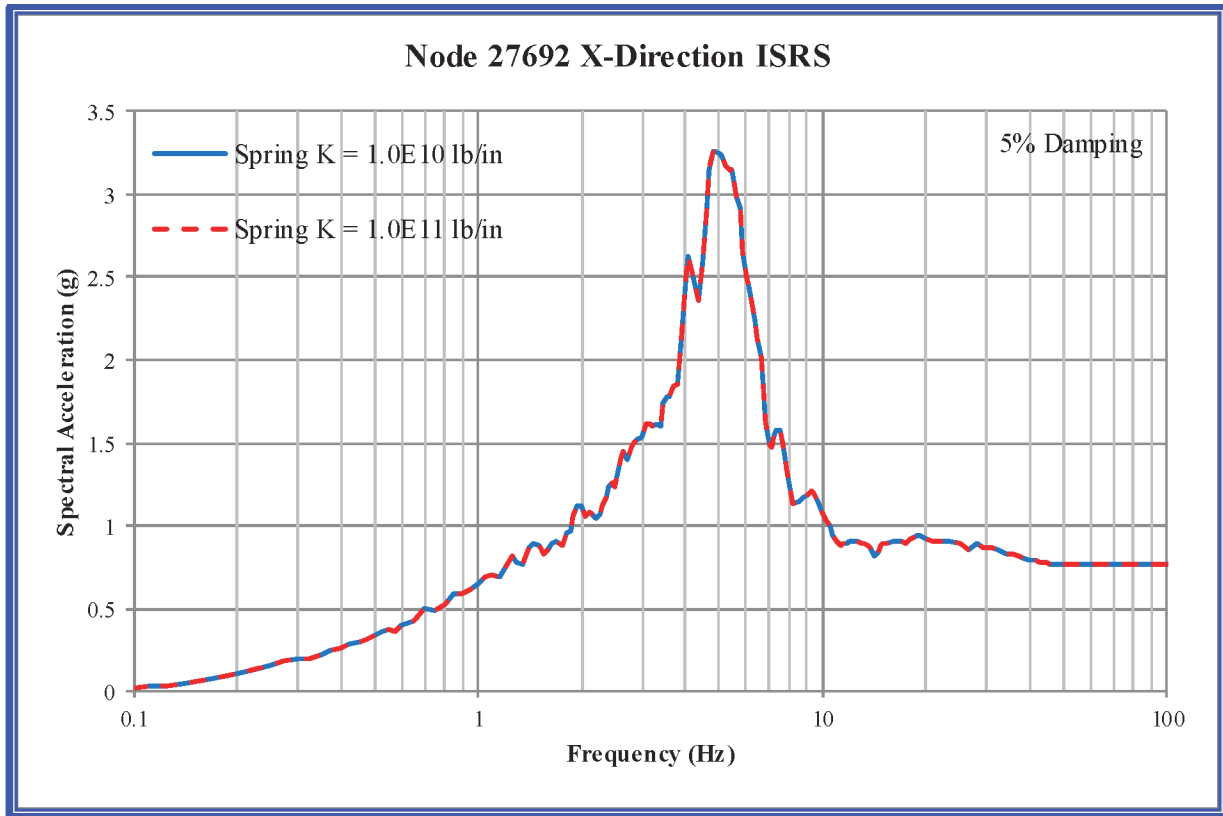


Figure 1-29. RXB - East-West (X) ISRS, Node 27692, Crane Rail Slab between Grid Lines RX-4 and RX-5 at El. 145'-6", Capitola Input.

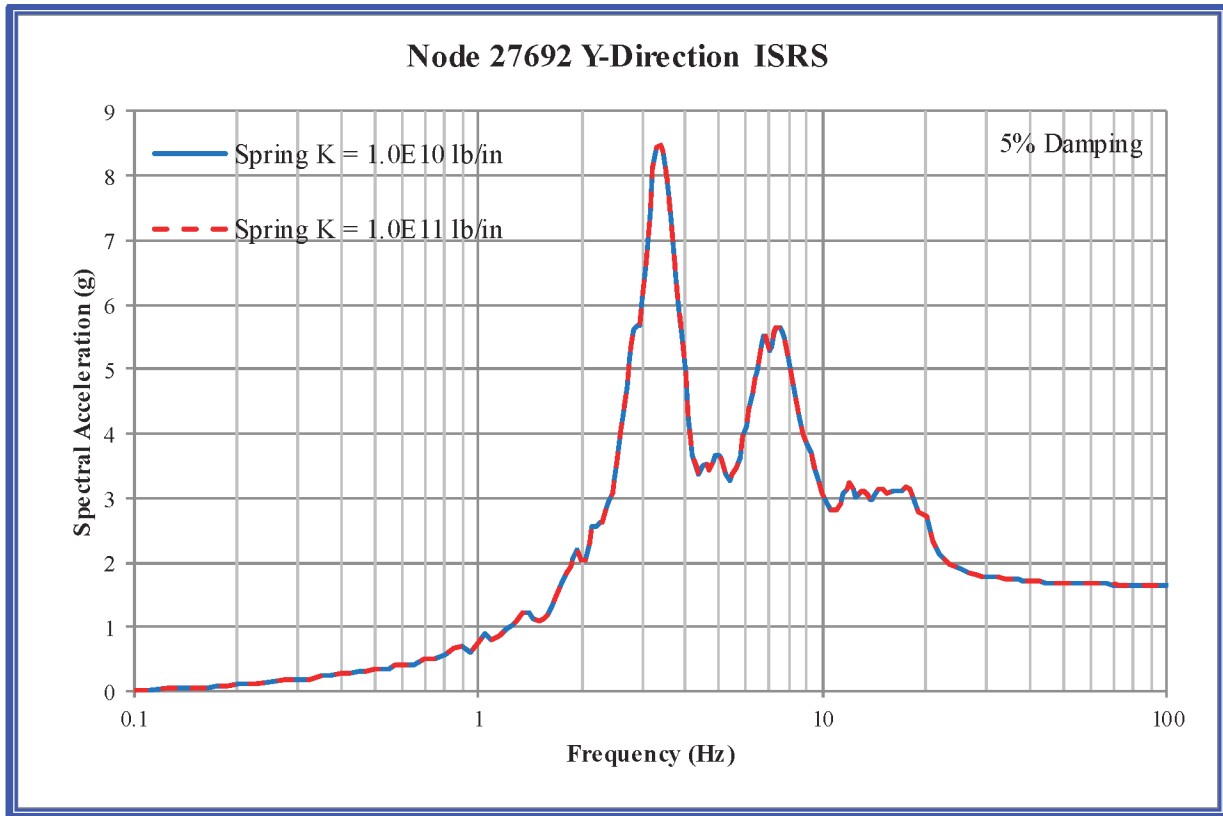


Figure 1-30. RXB - North-South (Y) ISRS, Node 27692, Crane Rail Slab between Grid Lines RX-4 and RX-5 at El. 145'-6", Capitola Input.

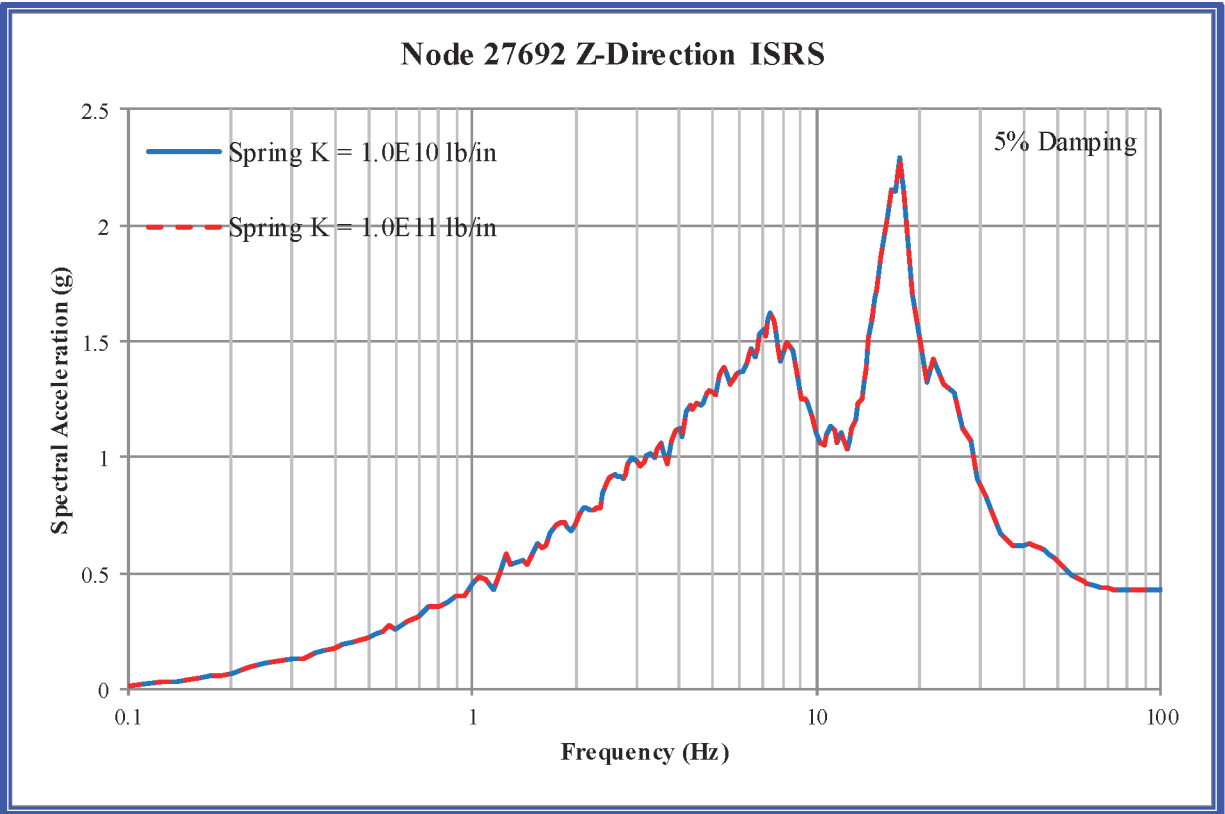


Figure 1-31. RXB - Vertical (Z) ISRS, Node 27692, Crane Rail Slab between Grid Lines RX-4 and RX-5 at El. 145'-6", Capitola Input.

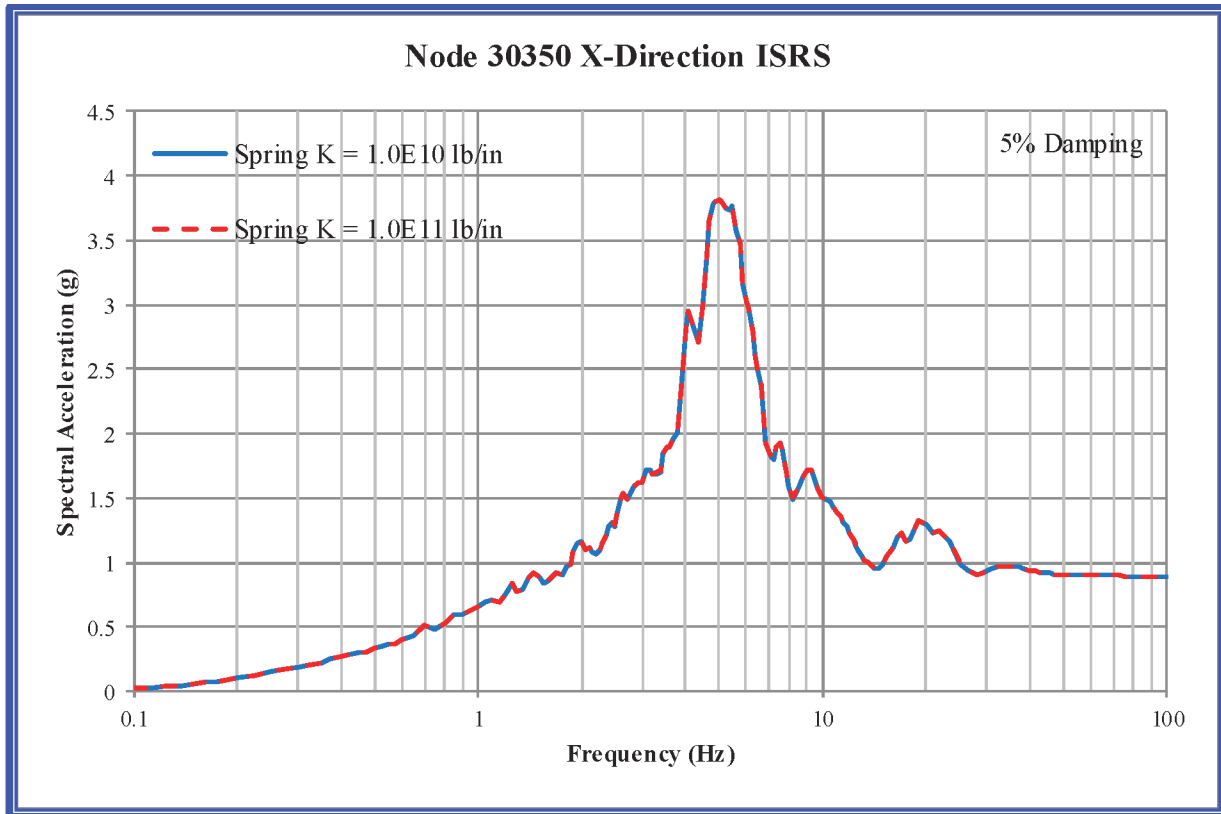


Figure 1-32. RXB - East-West (X) ISRS, Node 30350, Roof Slab between Grid Lines RX-4 and RX-5, Capitola Input.

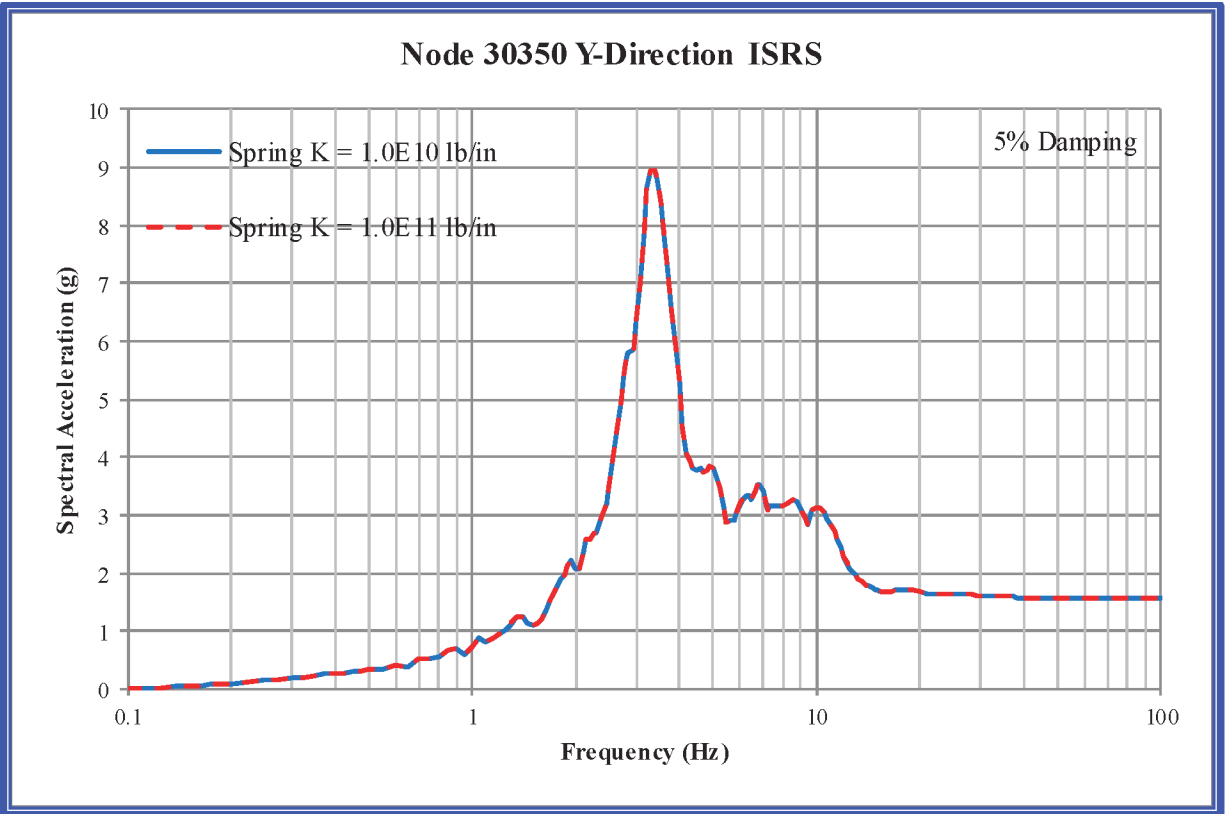


Figure 1-33. RXB - North-South (Y) ISRS, Node 30350, Roof Slab between Grid Lines RX-4 and RX-5, Capitola Input.

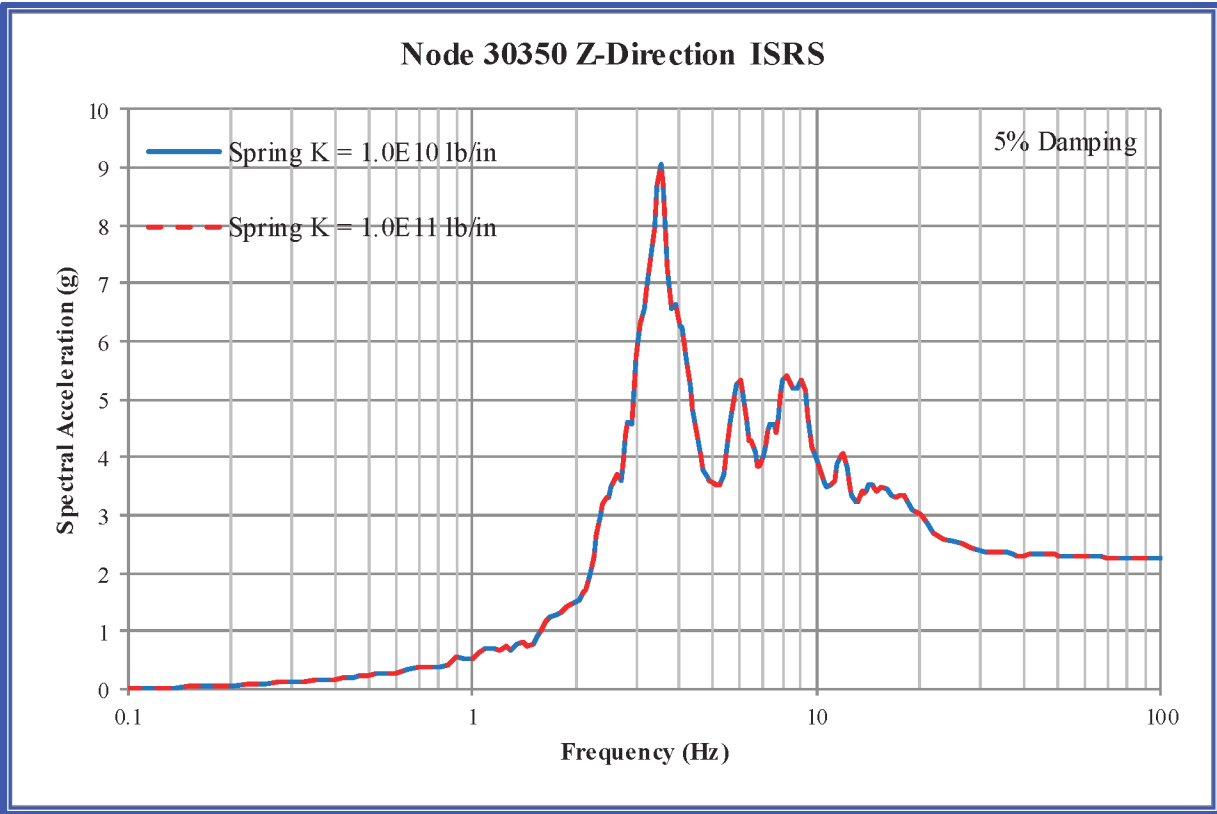


Figure 1-34. RXB - Vertical (Z) ISRS, Node 30350, Roof Slab between Grid Lines RX-4 and RX-5, Capitola Input.

1.3 Total Spring Forces

In this section, the sum of the maximum forces in all 4,470 rigid spring elements is compared. The maximum forces in the rigid springs due to the three input directions have been combined using the SRSS method.

The cracked concrete model with 7% concrete damping was used to generate these results. Results are presented for the Capitola input case.

Table 1-2 contains the sum of the maximum spring forces in all of the rigid springs elements for the cases with spring $K=10^{10}$ lb/in and spring $K=10^{11}$ lb/in and the percent difference being calculated as: $|\frac{K=10^{11} - K=10^{10}}{K=10^{10}} \times 100|$. This table shows that the largest percent difference between the two cases is 0.17%, in the Y (NS) direction.

The average of the percent difference of the forces over all of the rigid spring elements is provided in Table 1-3. The largest average percent difference is 0.29%, in the X (EW) and Y (NS) directions.

Table 1-2. Sum of Maximum Spring Forces in All Rigid Spring Elements, Capitola Input.

Direction	Total of Maximum Spring Force (kips)		
	Spring K = 10 ¹⁰ lb/in	Spring K = 10 ¹¹ lb/in	Difference
X (EW)	1,071,556	1,071,494	0.01%
Y (NS)	1,406,865	1,404,451	0.17%
Z (VT)	1,670,423	1,669,582	0.05%

Table 1-3. Average Difference of Forces Over All Rigid Spring Elements, Capitola Input.

Direction	Difference
X (EW)	0.29%
Y (NS)	0.29%
Z (VT)	0.27%

1.4 Solid Element Stress Comparison

In this section, the stresses in solid elements 26 and 146 are compared. These elements were selected because they are attached to the rigid spring elements; Element 26 is a backfill soil element and Element 146 is a concrete basemat element. These elements are located in the bottom layer of solid elements and are shown in Figure 1-35. The maximum stresses due to the three input directions have been combined using the SRSS method.

The cracked concrete model with 7% concrete damping was used to generate these results. Results are presented for the Capitola input case.

Table 1-4 and Table 1-5 present the maximum stresses in Elements 26 and 146, respectively, for the cases with spring K=10¹⁰ lb/in and spring K=10¹¹ lb/in. The percent difference is calculated as: $[(K=10^{11}) - (K=10^{10})]/(K=10^{10}) \times 100$. The largest differences in stresses in Elements 26 and 146 are 0.61% and 0.25%, respectively.

The average of the percent difference of the stresses over all of the solid elements is provided in Table 1-6. The stress component σ_{yy} has the largest average percent difference of 0.22%.

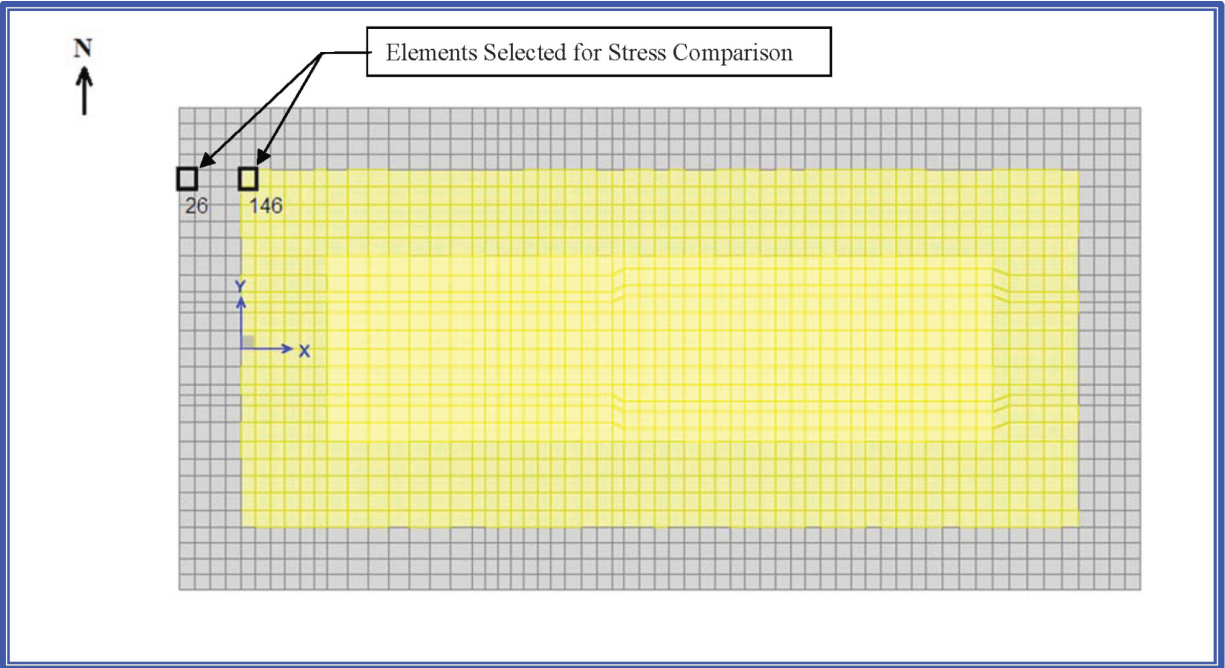


Figure 1-35. Plan View of Basemat Showing Location of Solid Elements 26 and 146.

Table 1-4. Comparison of Stresses in Solid Element 26, Capitola Input.

Stress Component	Element 26 Stress (psi)		
	Spring K= 10 ¹⁰ lb/in	Spring K= 10 ¹¹ lb/in	Difference
σ_{xx}	123.5	122.8	0.57%
σ_{yy}	130.6	129.8	0.61%
σ_{zz}	147.6	146.8	0.54%
τ_{xy}	2.1	2.1	0.00%
τ_{xz}	39.0	39.0	0.00%
τ_{yz}	5.1	5.1	0.00%

Table 1-5. Comparison of Stresses in Solid Element 146, Capitola Input.

Stress Component	Element 146 Stress (psi)		
	Spring K = 10 ¹⁰ lb/in	Spring K = 10 ¹¹ lb/in	Difference
σ_{xx}	235.6	235.0	0.25%
σ_{yy}	82.1	82.1	0.00%
σ_{zz}	194.1	194.1	0.00%
τ_{xy}	67.1	67.0	0.15%
τ_{xz}	91.6	91.8	0.22%
τ_{yz}	42.0	42.1	0.24%

Table 1-6. Average % Difference over All Solid Elements, Capitola Input.

Component	Difference
σ_{xx}	0.21%
σ_{yy}	0.22%
σ_{zz}	0.21%
τ_{xy}	0.09%
τ_{xz}	0.15%
τ_{yz}	0.15%

1.5 Beam Element Force and Moment Comparison

In this section, the forces and moments in beam elements 1304 and 5895 are compared. These elements were selected because they are on the outer wall. The locations of the elements are shown in Figure 1-36. The maximum forces and moments due to the three input directions have been combined using the SRSS method.

The cracked concrete model with 7% concrete damping was used to generate these results. Results are presented for the Capitola input case.

Table 1-7 and Table 1-8 present the maximum forces and moments in beam elements 1304 and 5895, respectively, for the cases with spring $K=10^{10}$ lb/in and spring $K=10^{11}$ lb/in. The percent difference is calculated as: $|(K=10^{11}) - (K=10^{10})| / (K=10^{10}) \times 100$.

The average of the percent difference of the forces and moments over all of the beam elements is provided in Table 1-9. The moments M2 and M3 have the largest average percent difference of 0.21%.

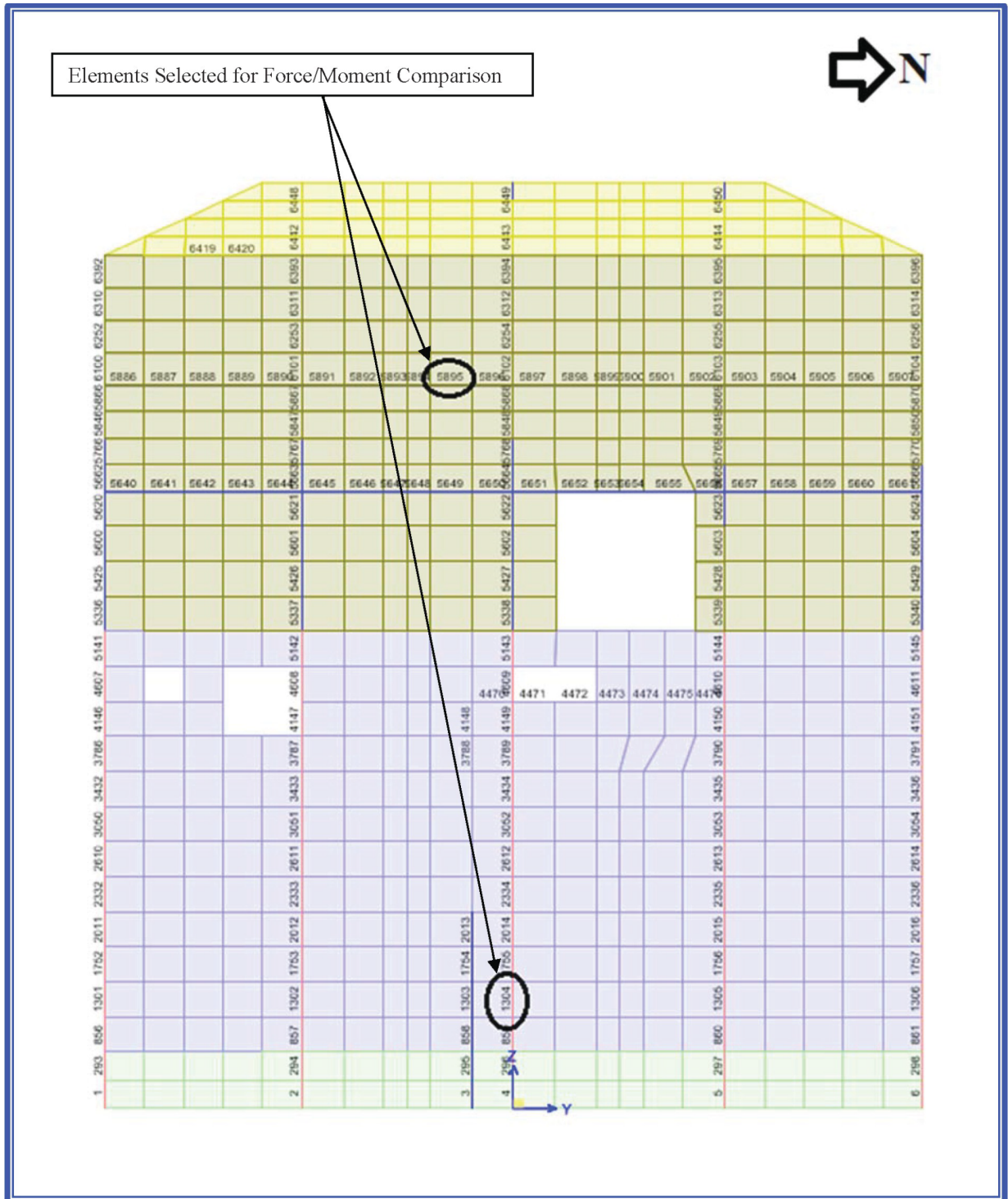


Figure 1-36. Elevation View of West Wall of RXB Looking West, Showing Location of Beam Elements 1304 and 5895.

Table 1-7. Comparison of Forces and Moments in Beam Element 1304, Capitola Input.

Component	Element 1304 Force/Moment		
	Spring K = 10 ¹⁰ lb/in	Spring K = 10 ¹¹ lb/in	Difference
P1 (k)	554.5	553.6	0.16%
P2 (k)	121.0	120.5	0.41%
P3 (k)	188.8	189.0	0.11%
M1 (k-ft)	72.7	72.6	0.14%
M2-I (k-ft)	2715.2	2716.9	0.06%
M2-J (k-ft)	1685.9	1686.7	0.05%
M3-I (k-ft)	1205.8	1215.3	0.78%
M3-J (k-ft)	1334.4	1335.9	0.11%

Table 1-8. Comparison of Forces and Moments in Beam Element 5895, Capitola Input.

Component	Element 5895 Force/Moment		
	Spring K = 10 ¹⁰ lb/in	Spring K = 10 ¹¹ lb/in	Difference
P1 (k)	1440.0	1441.0	0.07%
P2 (k)	85.0	85.0	0.00%
P3 (k)	191.8	191.7	0.05%
M1 (k-ft)	269.3	269.5	0.07%
M2-I (k-ft)	4903.9	4906.4	0.05%
M2-J (k-ft)	5172.1	5177.0	0.09%
M3-I (k-ft)	1139.3	1139.8	0.04%
M3-J (k-ft)	1472.8	1473.5	0.05%

Table 1-9. Average Difference Over All Beam Elements, Capitola Input.

Component	Difference
P1 (k)	0.13%
P2 (k)	0.07%
P3 (k)	0.09%
M1 (k-ft)	0.08%
M2 (k-ft)	0.21%
M3 (k-ft)	0.21%

1.6 Shell Element Force and Moment Comparison

In this section, the forces and moments in shell elements 3216 and 14620 are compared. These elements were selected because they are on the outer wall. The locations of the elements are shown in Figure 1-37. The maximum stresses due to the three input directions have been combined using the SRSS method.

The cracked concrete model with 7% concrete damping was used to generate these results. Results are presented for the Capitola input case.

Table 1-10 and Table 1-11 present the maximum forces and moments in Elements 3216 and 14620, respectively, for the cases with spring $K=10^{10}$ lb/in and spring $K=10^{11}$ lb/in. The percent difference is calculated as: $|(K=10^{11}) - (K=10^{10})| / (K=10^{10}) \times 100$.

The average of the percent difference of the forces and moments over all of the shell elements is provided in Table 1-12. The moment, M_{xy} , and shears, V_{xz} and V_{yz} , have the largest average percent difference of 0.07%.

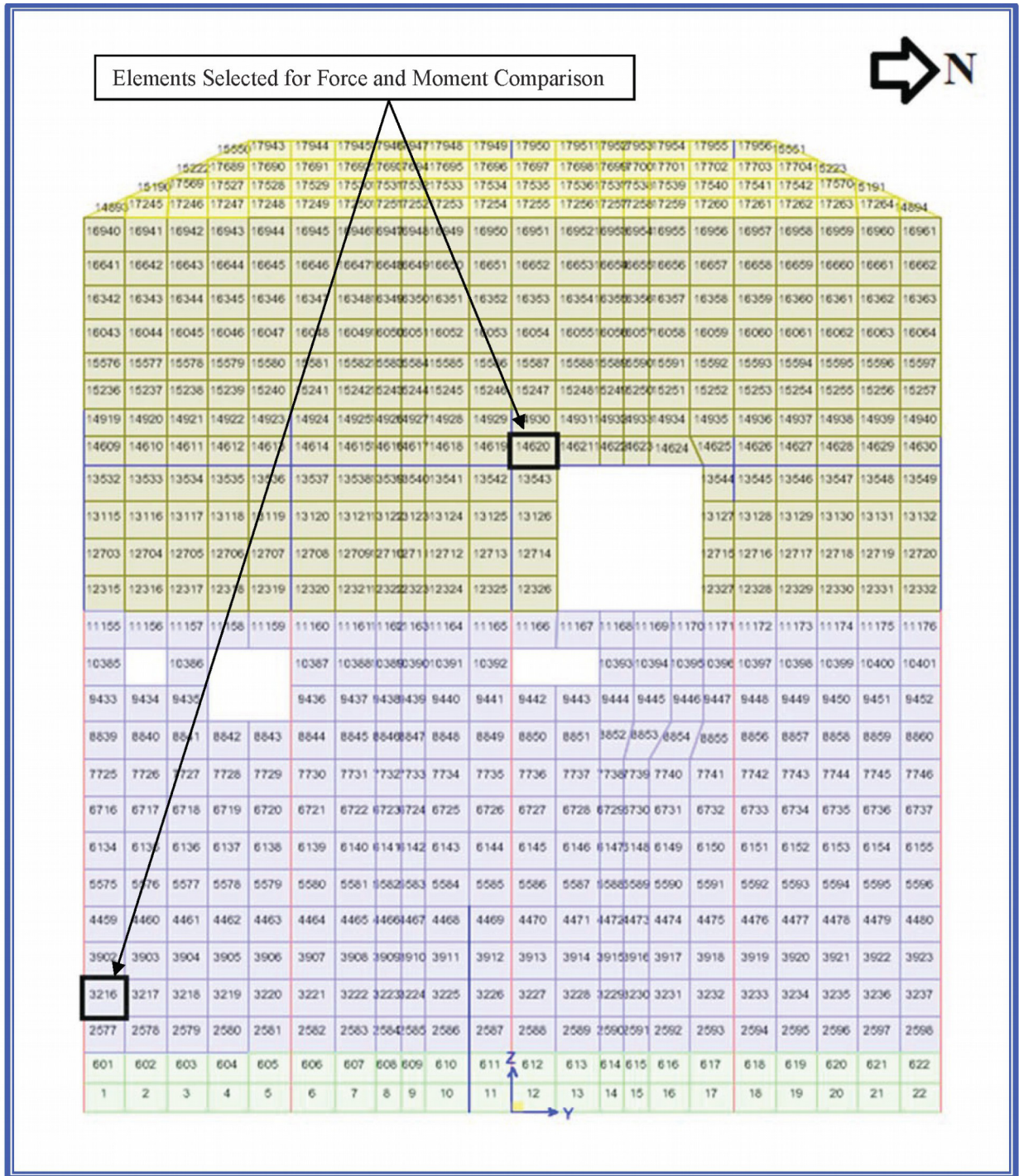


Figure 1-37. Elevation View of West Wall of RXB Looking West, Showing Location of Shell Elements 3216 and 14620.

Table 1-10. Comparison of Forces and Moments in Shell Element 3216, Capitola Input.

Element 3216 Force/Moment			
Component	Spring K = 10 ¹⁰ lb/in	Spring K = 10 ¹¹ lb/in	Difference
Sxx (k/ft)	43.6	43.6	0.00%
Syy (k/ft)	297.6	297.5	0.03%
Sxy (k/ft)	87.9	87.8	0.11%
Mxx (k-ft/ft)	54.6	54.7	0.18%
Myy (k-ft/ft)	15.1	15.1	0.00%
Mxy (k-ft/ft)	13.5	13.5	0.00%
Vxz (k/ft)	18.3	18.4	0.55%
Vyz (k/ft)	6.4	6.4	0.00%

Table 1-11. Comparison of Forces and Moments in Shell Element 14620, Capitola Input.

Element 14620 Force/Moment			
Component	Spring K = 10 ¹⁰ lb/in	Spring K = 10 ¹¹ lb/in	Difference
Sxx (k/ft)	305.2	305.0	0.07%
Syy (k/ft)	291.0	290.9	0.03%
Sxy (k/ft)	248.1	248.0	0.04%
Mxx (k-ft/ft)	24.7	24.7	0.00%
Myy (k-ft/ft)	17.2	17.2	0.00%
Mxy (k-ft/ft)	4.0	4.0	0.00%
Vxz (k/ft)	10.6	10.6	0.00%
Vyz (k/ft)	9.0	9.0	0.00%

Table 1-12. Average Difference Over All Shell Elements, Capitola Input.

Component	Difference
Sxx (k/ft)	0.06%
Syy (k/ft)	0.06%
Sxy (k/ft)	0.05%
Mxx (k-ft/ft)	0.06%
Myy (k-ft/ft)	0.06%
Mxy (k-ft/ft)	0.07%
Vxz (k/ft)	0.07%
Vyz (k/ft)	0.07%

c.

Most elements in the RXB model mesh were square, i.e., had an aspect ratio close to 1.0. The aspect ratio of 11.9 was for non-structural, surface elements. As demonstrated in the response to RAI 8932, Question 03.07.02-1, mesh size has negligible effect on the behavior and results of the model. Verification and validation of SASSI, including aspect ratio, will be provided with the response to RAI 8936, Question 3.07.02-7S1.

Impact on DCA:

FSAR Tier 2, Section 3.7.2.1.2.1 and Table 3.7.2-1 have been revised as described in the response above and as shown in the markup provided in this response.

beam elements in red. Figure 3.7.2-21 shows all beam elements in the SASSI2010 model.

The free field soil is defined such that the RXB with backfill soil can fit exactly to the 'pit' in the excavated soil halfspace. The connectivity between the RXB with backfill soil and the excavated free field soil is achieved by connecting the skin nodes of the excavated soil model with the nodes on the embedded skin of the RXB with backfill model using rigid soil springs. The skin nodes of the excavated soil model and the skin nodes of the RXB with backfill model have identical coordinates, and they are in one-to-one correspondence matching pairs.

RAI 03.07.02-17

The rigid springs have a zero length and have a stiffness value large enough to simulate rigid connection. The large stiffness used is arbitrarily chosen to be ten billion lbs per inch, or 10^{10} lbs/inch, in the three global directions. [A sensitivity analysis was performed by increasing the stiffness of the RXB rigid springs by an order of magnitude, to \$10^{11}\$ lb/in, and comparing results obtained from the base case, rigid spring stiffness of \$10^{10}\$ lb/in. For this study, the RXB model with cracked concrete properties, 7 percent concrete damping, Soil Type 7, and the Capitola input motion, was used. Comparisons of transfer functions and ISRS show that increasing the rigid spring stiffness has no discernible effect on the transfer functions and ISRS.](#)

The model dimensions, the quantities of elements and masses, and structural damping ratios used for the SASSI2010 model are summarized in Table 3.7.2-1.

The NPMs and the Reactor Building crane (RBC) are included in the RXB model as beam models. These two subsystems are discussed in the following sections.

RAI 03.08.05-12S2

The reactor building basemat is designed using a combination of different models. First, the structural responses from the building models are extracted. Then they are applied to separate basemat models to determine structural design forces and moments for the basemat. Table 3.7.2-49 and Table 3.7.2-50 show which models are used, what results are extracted, and how these results are used to design the basemat.

3.7.2.1.2.2

NuScale Power Modules

Up to twelve NPMs will be inside the RXB. The modules are partially immersed in the reactor pool. The NPMs are not permanently bolted or welded to the pool floor or walls. Instead they are geometrically supported and constrained at four locations. The geometrical constraints are designed to keep each NPM in its location before, during, and after a seismic event.

The base support is a steel skirt that rests outside a permanently installed ring plate attached at the bottom of the reactor pool. The other three geometrical supports are steel lug restraints located on the walls of each bay at

RAI 03.07.02-17

Table 3.7.2-1: Summary of Reactor Building SASSI2010 Model

Model Portions	Description	
Overall model dimensions	391' long (East-West), 195.5' wide (North-South), 165' high, embedded 86' deep	(n/a)
General	Number of lumped masses [†]	30,568
	Concrete structural damping for calculation of acceleration responses for ISRS generation (percent)	4
	Concrete structural damping for calculation of member forces and moments for structural design (percent)	7
RXB (including Backfill Soil)	Total number of nodes	30,762
	Backfill soil solid elements	9,236
	Foundation mat solid elements	2,839
	Beam elements	6,453
	Plate elements	18,818
	Spring elements modeling NPM support stiffness	1,114
	Fraction of quadrilateral and triangular elements (%)	2.45
	Typical element size (ft)	6
	Maximum element size (ft)	12
	Typical aspect ratio	1.29
	Maximum aspect ratio [*]	11.9
Connection between RXB and excavated soil	7P interaction nodes for extended subtraction method	7,950
	Rigid springs connecting RXB and excavated free-field soil	4,470
Excavated soil	Excavated soil nodes	28,830
	Excavated soil solid elements	25,620

Notes: † All masses are assigned as assembled joint lumped masses at each node.

*The aspect ratio of 11.9 is for a small number of non-structural, surface elements.